

Emergenet: A Digital Twin of Sequence Evolution for Scalable Emergence Risk Assessment of Animal Influenza A Strains

Kevin Yuanbo Wu¹, Jin Li¹, Aaron Esser-Kahn^{2,3}, and Ishanu Chattopadhyay^{1,4,5}*

¹Department of Medicine, University of Chicago, IL, USA

²Pritzker School of Molecular Engineering, University of Chicago, Chicago, IL, USA

³Committee on Immunology, University of Chicago, Chicago, IL, USA

⁵Committee on Quantitative Methods in Social, Behavioral, and Health Sciences, University of Chicago, IL, USA

*To whom correspondence should be addressed: e-mail: ishanu@uchicago.edu.



Abstract: Despite having triggered devastating pandemics in the past, our ability to quantitatively assess the emergence potential of individual strains of animal influenza viruses remains limited. This study introduces Emergenet, a tool to infer a digital twin of sequence evolution to chart how new variants might emerge in the wild. Our predictions based on Emergenet's built only using 220,151 Hemagglutinin (HA) sequences consistently outperform WHO seasonal vaccine recommendations for H1N1/H3N2 subtypes over two decades (average match-improvement: 3.73 AAs, 28.40%), and are at par with state-of-the-art approaches that use more detailed phenotypic annotations. Finally, our generative models are used to scalably calculate the current odds of emergence of animal strains not yet in human circulation, which strongly correlates with CDC's expert-assessed Influenza Risk Assessment Tool (IRAT) scores (Pearson's $r = 0.721, p = 10^{-4}$). A minimum five orders of magnitude speedup over CDC's assessment (seconds vs months) then enabled us to analyze 6,354 animal strains collected post-2020 to identify 35 strains with high emergence scores (> 7.7). The Emergenet framework opens the door to preemptive pandemic mitigation through targeted inoculation of animal hosts before the first human infection.

Introduction

Influenza viruses constantly evolve⁵, sufficiently altering surface protein structures to evade the prevailing host immunity, and cause the recurring seasonal epidemic. These periodic infection peaks claim a quarter to half a million lives⁶ globally, and currently our response hinges on annually inoculating the human population with a reformulated vaccine^{5,7}. Among numerous factors that hinder optimal design of the flu shot, failing to correctly predict the future frequency-dominant strains dramatically reduces vaccine effectiveness⁸. Despite recent advances^{6,9} such predictions remain imperfect. In addition to the seasonal epidemic, influenza strains spilling over into humans from animal reservoirs have triggered pandemics at least four times (1918 Spanish flu/H1N1, 1957 Asian flu/H2N2, 1968 Hong Kong flu/H3N2, 2009 swine flu/H1N1) in the past 100 years¹. With the memory of the sudden SARS-CoV-2 emergence fresh in our minds, a looming question is whether we can preempt and mitigate such events in the future. Influenza A, partly on account of its segmented genome and its wide prevalence in common animal hosts, can easily incorporate genes from multiple strains and (re)emerge as novel human pathogens^{3,10}.

One possible approach to mitigating such risk is to identify animal strains that do not yet circulate in humans, but is likely to spill-over and quickly achieve human-to-human (HH) transmission capability. While global surveillance efforts collect wild specimens from diverse hosts and geo-locations annually, our ability to objectively, reliably and scalably risk-rank individual strains remains limited¹², despite some recent progress¹³⁻¹⁵.

The Center for Disease Control's (CDC) current solution to this problem is the Influenza Risk Assessment Tool (IRAT)¹⁶. Subject matter experts (SME) score strains based on the number of human infections, infection and transmission in laboratory animals, receptor binding characteristics, population immunity, genomic analysis, antigenic relatedness, global prevalence, pathogenesis, and treatment options, which are averaged to obtain two scores (between 1 and 10) that estimate 1) the emergence risk and 2) the potential public health impact on sustained transmission. IRAT scores are potentially subjective, and depend on multiple experimental assays, possibly taking weeks to compile for a single strain. This results in a scalability bottleneck, particularly with thousands of strains being sequenced annually.

Here we introduce a pattern recognition algorithm to automatically parse out emergent evolutionary constraints operating on Influenza A viruses in the wild, to provide a less-heuristic, theory-backed scalable solution to emergence

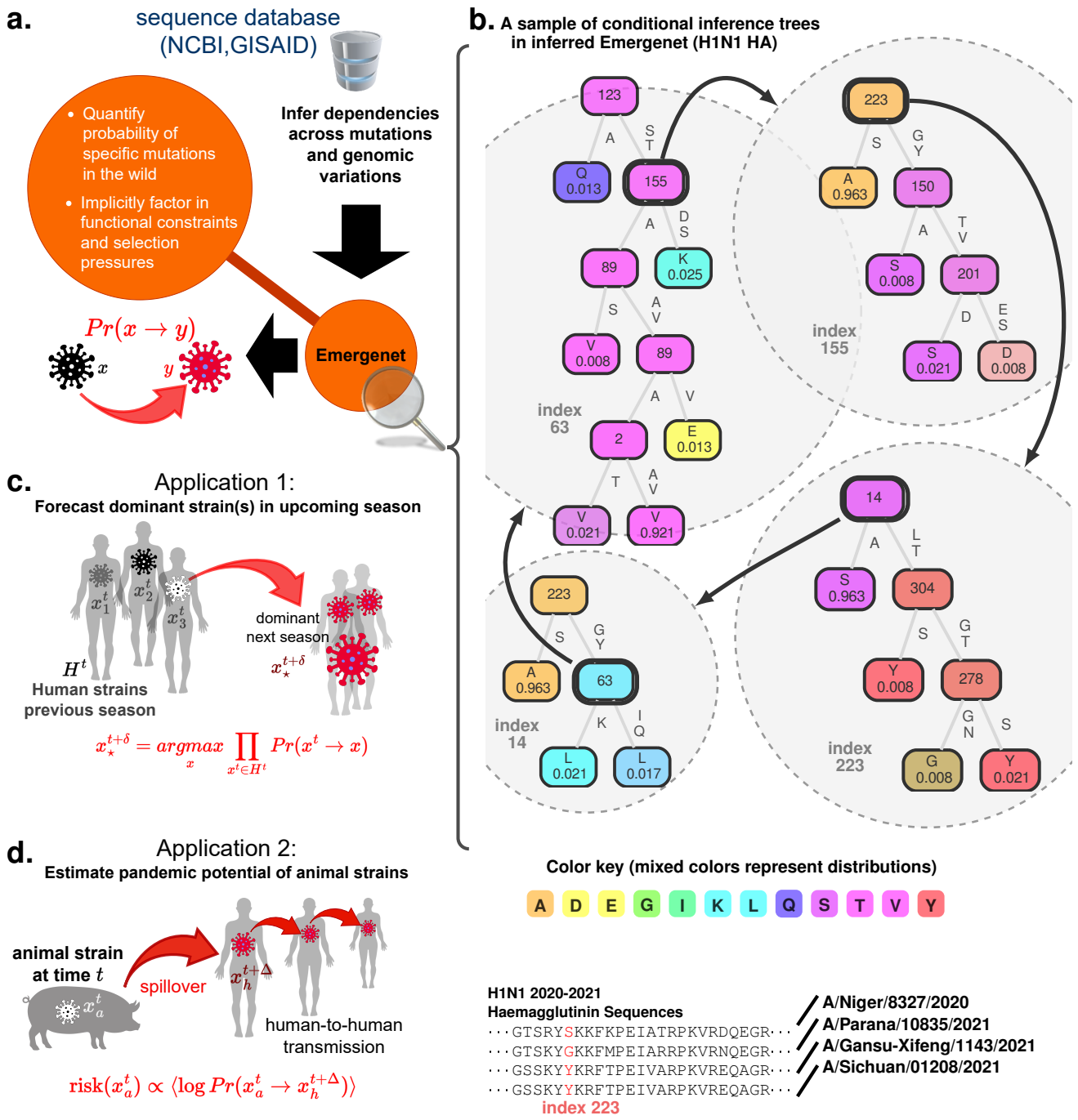


Fig. 1. Emergenet inference and applications. Panel a Variations of genomes for identical subtypes of Influenza A are analyzed to infer a recursive forest of conditional inference trees¹¹ – the Emergenet – which maximally captures the emergent dependencies between an a priori unspecified number of mutations. With these inferred dependencies we can estimate the numerical odds of specific mutations, and by extension, the numerical value of the probability of one strain giving rise to another in the wild, under complex selection pressures from the background. Panel b Snapshot of decision trees from the Emergenet inferred for H1N1 HA sequences collected in 2020-2021, which reveals a cyclic dependency. In general, every internal node of a component tree can be “expanded” into its own tree, underscoring the recursive structure of the Emergenet. Panel c First application: forecast dominant strain(s) for the next flu season, using only sequences collected up to six months prior and the inferred Emergenet, using data from the past year. Panel d Second application: estimation of the pandemic risk posed by individual animal strains that are still not known to circulate in humans.

prediction. Our approach is centered around numerically estimating the probability $Pr(x \rightarrow y)$ of a strain x giving rise to y which is well-adapted to humans. We show that this capability is key to preempting strains which are expected to be in future circulation, and approximate IRAT scores of non-human strains without experimental assays or SME scoring.

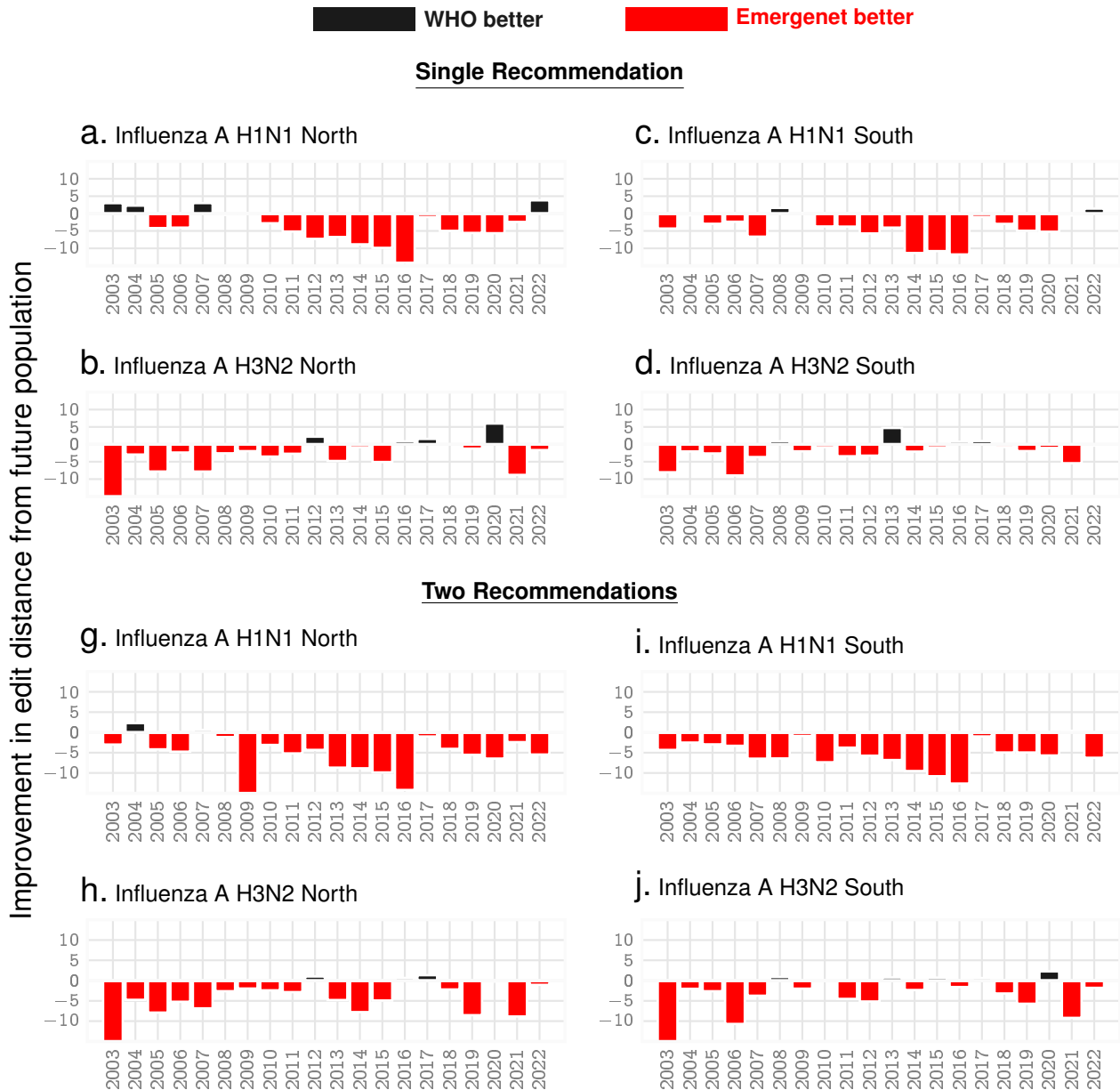


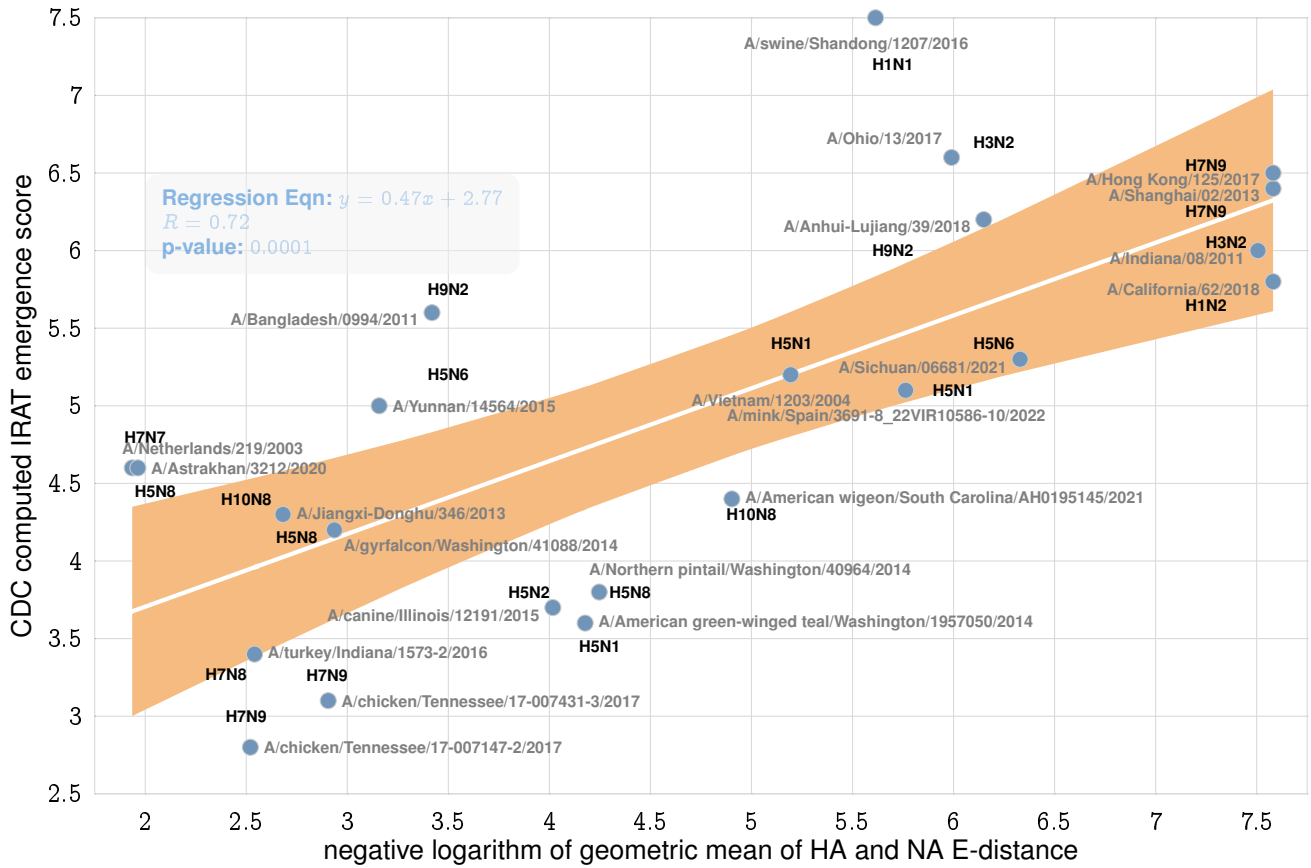
Fig. 2. **Seasonal predictions for Influenza A.** Relative out-performance of Emergenet predictions against WHO recommendations for H1N1 and H3N2 subtypes for Hemagglutinin (HA) over the both hemispheres. The negative bars (red) indicate the reduced average Hamming distance between the predicted sequence and the sequence population that season. Providing two recommendations shows a significant improvement over providing a single recommendation. Note that the recommendations for the north are given in February, while that for the south are given in September, keeping in mind that the southern flu season begins a few months earlier (e.g. for the 2022-2023 flu season, northern data is labelled '2022').

Emergenet: Digital Twin of Sequence Evolution in the Wild

To uncover relevant evolutionary constraints, we analyze variations (point substitutions and indels) of the residue sequences of key proteins implicated in cellular entry and exit^{1,17}, namely HA and NA respectively. By capturing the emergent cross-dependencies between these sequence variations our model, the Emergenet (Enet), estimates the odds of a specific mutation to arise in future, and consequently the probability of a specific strain evolving into another (Fig. 1a). Our calculations are based on first inferring the variation of mutational probabilities, and the potential residue replacements which vary along a sequence. The many well-known classical DNA substitution models¹⁸ or standard phylogeny inference tools which assume a constant species-wise mutational characteristics, are not applicable here. Similarly, newer algorithms such as FluLeap¹⁹ which identifies host tropism from sequence data, or estimation of species-level risk¹⁵ do not allow for strain-specific assessment.

The dependencies we uncover are shaped by a functional necessity of conserving/augmenting fitness. Strains must be sufficiently common to be recorded, implying that the sequences from public databases that we train with have high replicative fitness. Lacking kinetic proofreading, Influenza A integrates faulty nucleotides at a relatively high rate ($10^{-3} - 10^{-4}$) during replication^{20,21}. However, few variations are actually viable, manifesting discernible dependencies

a. Predicted emergence risk vs published IRAT scores



b. Global prediction of IRAT scored for all Influenza A sequences collected since 2020

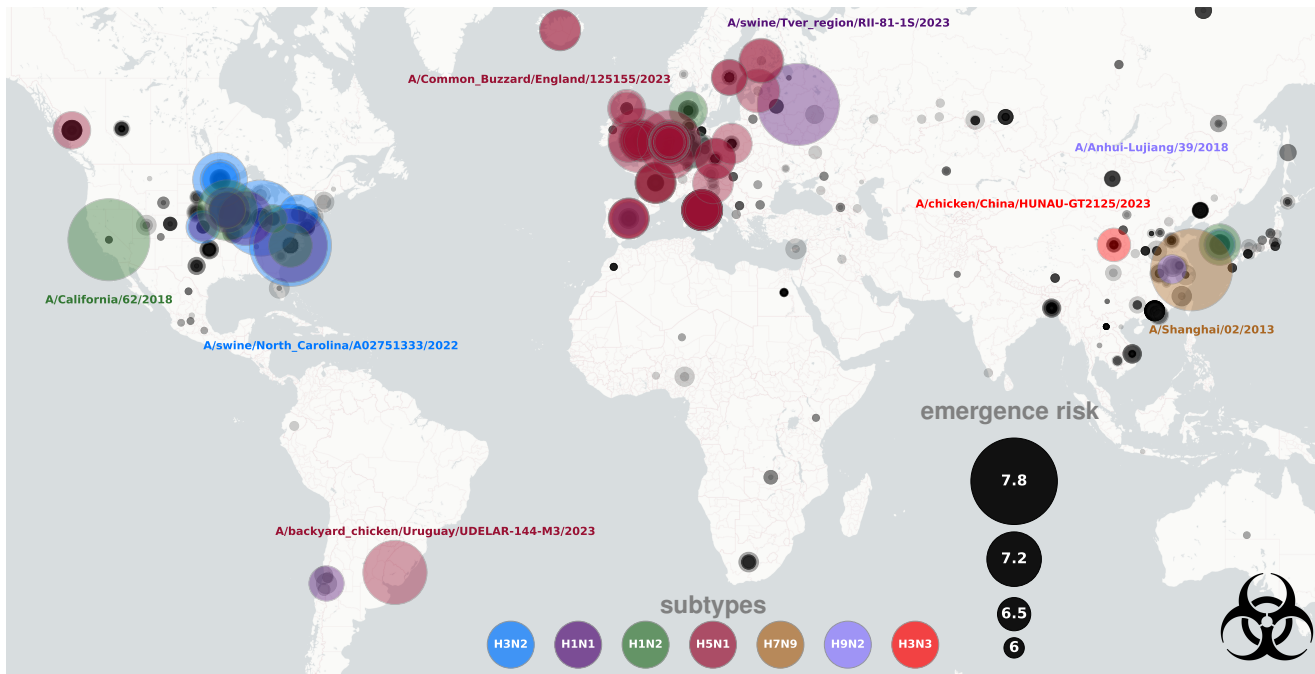


Fig. 3. **Emergenet based estimation of IRAT scores for animal strains.** Panel a We find an approximate linear relationship between the negative logarithm of the geometric mean of the smallest E-distance for HA and NA sequence of a target strain from circulating human strains in the year of estimation and the CDC published IRAT emergence scores. Panel b Identifying risky Influenza A strains amongst those collected 2020-2023 using our approach.

between such mutations. These fitness constraints also vary over time. The background strain distribution, and selection pressure from the evolution of cytotoxic T lymphocyte epitopes²²⁻²⁶ in humans can change quickly. However, with a sufficient number of unique samples to train on for each flu season, the Emergenet (recomputed for each time-period) is expected to automatically factor in the evolving host immunity, and the current background environment.

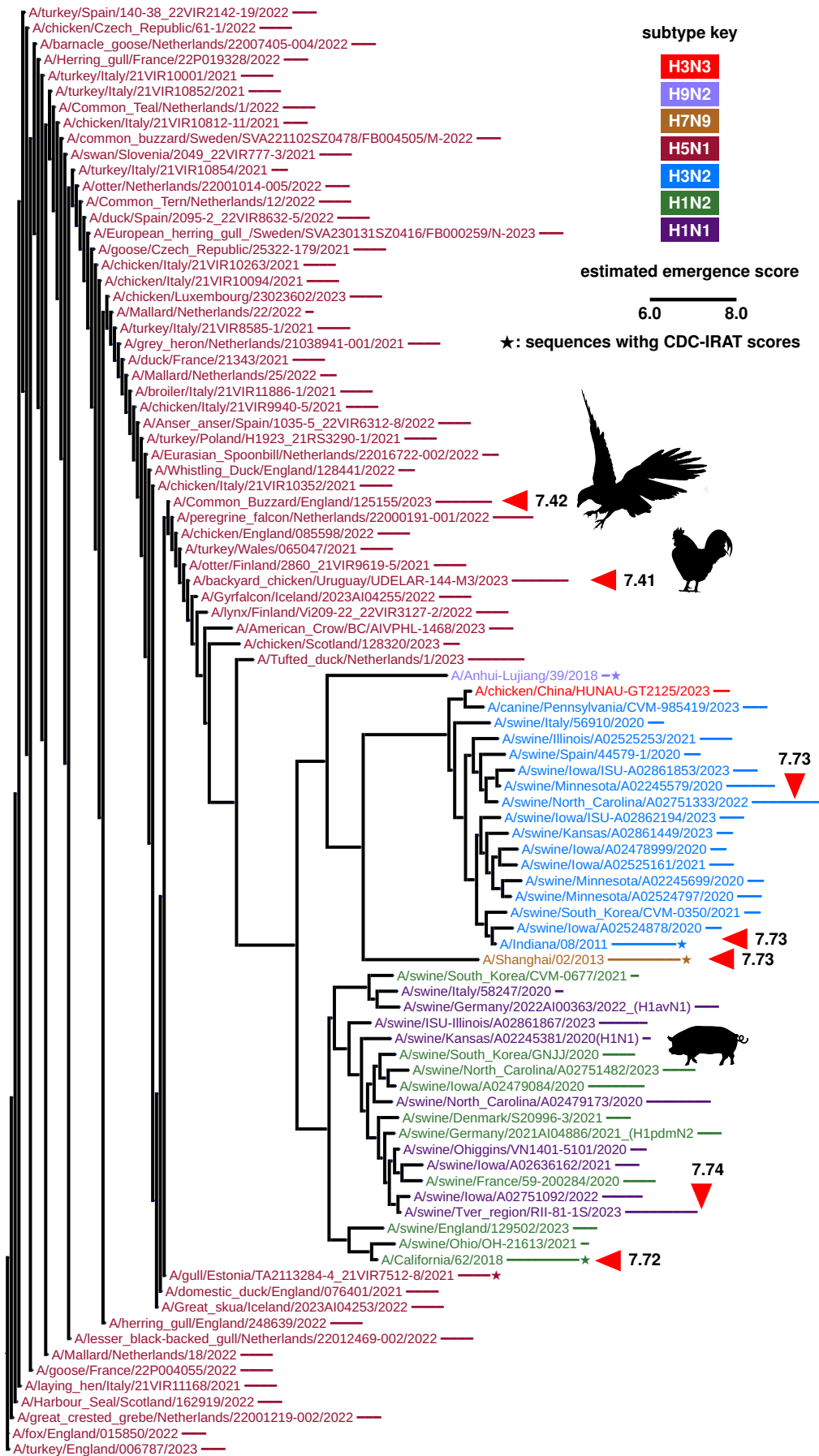
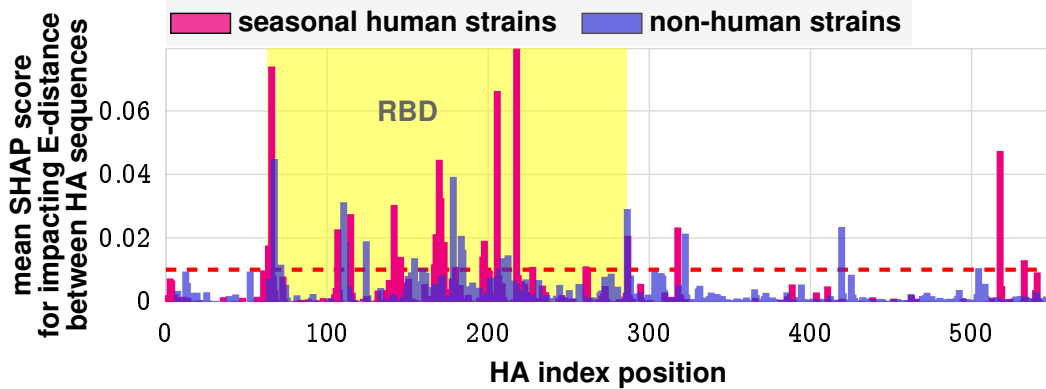


Fig. 4. Phylogeny constructed with edit distances, with all Influenza A strains collected post 2020, with estimated IRAT emergence risk > 6.0. Strains with CDC-computed IRAT scores are also included (shown with ★). Leaves have been collapsed which differ by less than 20 edits in the HA, displaying the most risky strains in the collapsed group, which comes from diverse animal hosts, and geographic regions. Top strains are indicated by arrowheads.

a. Importance score of positional indices in strain similarity



b. Highlighting residues critical for E-distance modulation ($SHAP > 0.01$), human strains (left) and high-risk animal strains (right)

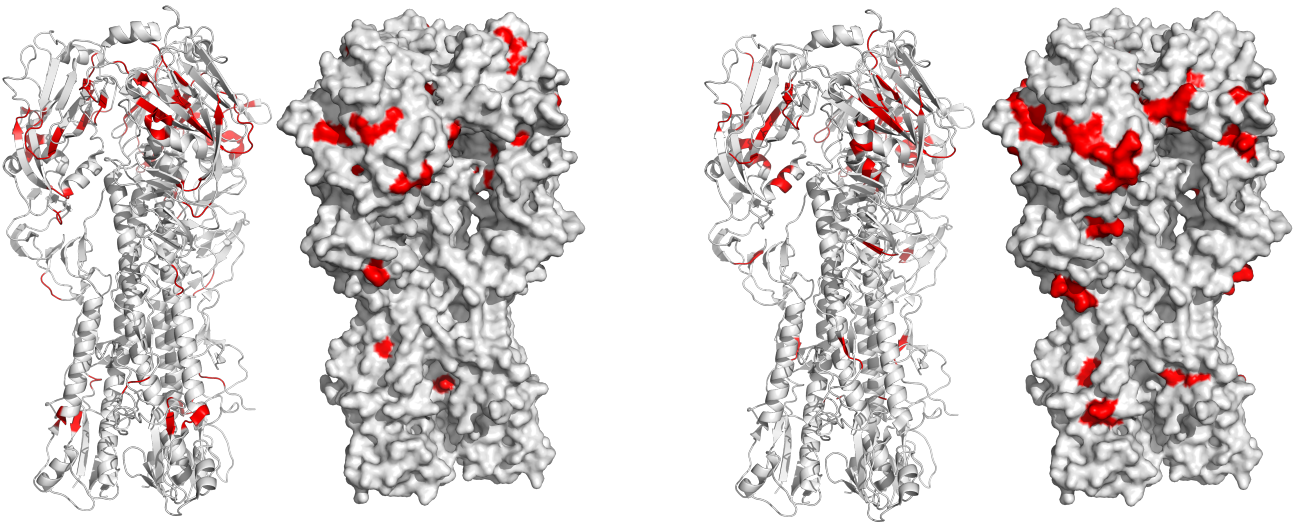


Fig. 5. **SHAP analysis of RBD.** Using a SHAP analysis we quantify the relative importance of individual residues in modulating the E-distance between two HA sequences, on average. **Panel a** The residues within the RBD is clearly having more impact for both seasonal Influenza A strains and high-risk animal strains (high-risk as determined by IRAT). **Panel b** Visualizing the residues on the molecular structure of HA (approximate, uses the same atom positions for all renderings (1ruz.pdb)), we find that the high SHAP residues (high importance in modulating E-distance between strains) are largely localized near the globular head domain, and have surface exposure. We also note that the seasonal and animal strains have similar but distinct high-value residues.

Structurally, an Emergenet comprises an interdependent collection of local predictors, each aiming to predict the residue at a particular index using as features the residues at other indices (Fig. 1b). Thus, an Emergenet comprises almost as many such position-specific predictors as the length of the sequence. These individual predictors are implemented as conditional inference trees¹¹, in which nodal splits have a minimum pre-specified significance in differentiating the child nodes. Thus, each predictor yields an estimated conditional residue distribution at each index. The set of residues acting as features in each predictor are automatically identified, *e.g.*, in the fragment of the H1N1 HA Emergenet (2020-2021, Fig. 1b), the predictor for residue 63 is dependent on residue 155, and the predictor for 155 is dependent on 223, the predictor for 223 is dependent on 14, and the residue at 14 is again dependent on 63, revealing a cyclic dependency. The complete Emergenet harbors a vast number of such relationships, wherein each internal node of a tree may be “expanded” to its own tree. Owing to this recursive expansion, a complete Emergenet substantially captures the complexity of the rules guiding evolutionary change as evidenced by our out-of-sample validation.

Before we apply our approach to quantifying risk from animal strains, we demonstrate identification of vaccine strains for the seasonal flu epidemics, with only sequence information, with performance at par with approaches using deep mutational scanning (DMS) assays⁶.

For that purpose, we used H1N1 and H3N2 HA sequences from Influenza A strains in the public NCBI and GISAID databases recorded between 2001-2023 (220,151 in total, Supplementary Table S-1). We construct Emergenets separately for both subtypes, yielding 84 models for predicting seasonal dominance. The Emergenet predictors induce an intrinsic distance metric (E-distance) between strains (Eq. (8) in Methods & Materials), defined as the square-

root of the Jensen-Shannon (JS) divergence²⁸ of the conditional residue distributions, averaged over the sequence. Unlike the classical approach of measuring the number of edits between sequences, the E-distance is informed by the Emergenet-inferred dependencies, and adapts to the specific subtype, allele frequencies, and environmental variations. We show (Theorem 1 in Methods & Materials) that the E-distance scales as the log-likelihood of spontaneous change *i.e.* $\log Pr(x \rightarrow y)$.

Phenotypic differences are often driven by specific loci, and antigenic differences in influenza are typically strongly affected by changes within the receptor binding domain (RBD)^{29,30}. With the complex cross-talk between loci uncovered by the Emergenet, evaluating the impact of individual loci in modulating phenotypic characteristics becomes non-trivial. We investigated the relative importance of specific loci in modulating the E-distance between strains, and consequently phenotypic changes, via a standard SHAP analysis^{31,32} (Fig. 5). Such analyses, rooted in cooperative game theory, has been successfully used in the literature to uncover average impact of individual inputs in complex machine learning models³³. We first estimate the impact of each residue in determining the E-distance between a given strain, and a “consensus” strain, and then calculate the average impact of the individual residues over a representative set of strains. Our results indicate that in both seasonal analysis and emergence risk of animal strains, we have 1) a complex distribution of important residues along the HA sequence, 2) residues within the RBD are clearly playing dominant roles (Fig. 5a), 3) relatively few residues among the 566 possible locations are driving most of the effect (Fig. 5b).

As a baseline comparison without using SHAP analysis, we also estimated the correlation of E-distance between animal and common human strains (Extended Data Table 11), which shows that edit distance on the RBD is strongly correlated to E-distance, both for the CDC-analyzed strains and animal strains collected within 2020-2022 period, but were not informative or trended incorrectly when we looked at selected individual residues of known functional relevance, suggesting complicated impact sharing by individual loci.

Note that despite general correlation between E-distance and edit-distance, the E-distance between fixed strains can change if only the background environment changes (Supplementary Table S-2, S-3) with the strains remaining unchanged. Thus, we re-learn models using recent historical circulation, and only predict for the near future. In in-silico experiments, we find that while random mutations to genomic sequences produce rapidly diverging sets, Emergenet-constrained replacements produce verifiably meaningful sequences (See “In-silico Corroboration of Emergenet’s Capability To Capture Biologically Meaningful Structure” in Methods & Materials and Supplementary Fig. S-4).

We then investigated how sampling of the observed strains, which naturally arises by how strains are collected, affects model training (Supplementary Fig. S-5). Fixing a particular time-period (2018-19 northern hemisphere shown), we trained 100 Emergenet models with different random samples of 3000 strains, picked two random strains from two of the largest clusters, and computed their E-distance under each of the 100 models. We see that the E-distances are relatively stable, with distances between two strains in the same cluster substantially smaller than the inter-cluster distances, demonstrating model stability (and that cluster identity is largely preserved under such variations). Later we also investigate that the uncertainty from the limited sampling of animal strains leads to small standard error of mean (SEM) in the estimated emergence scores.

Finally, we note that while learning a precise model of jump from one strain to another is infeasible from the available data, our approach can feasibly uncover a subset of the transition rules that are best supported by statistical evidence, allowing us to probabilistically constrain the set of future possibilities. Viewing each locus in the sequence individually as a target variable, and using all other loci as features to obtain a classification model, results in ≤ 566 conditional inference trees (for HA), as described above. Using conditional inference trees for the individual classification models implies that only statistically significant splits are allowed in the inferred decision trees. When no such splits are found, we do not return a classification model for that index. Finally, this forest of trees collectively comprise a Emergenet model. Each such model induces a distance metric between strains, referred to as the E-distance metric, which is shown (Theorem 1 in Methods & Materials) to scale with the log-likelihood of the jump probability. Estimating the numerical odds of a jump $Pr(x \rightarrow y)$ (Fig. 1) allows us to derive quantitative solutions to the problem of forecasting vaccine strain(s), and that of estimating the emergence potential of an animal strain (Fig. 1c-d, Eq. (1)-(4)).

Predicting Seasonal Vaccine Strains

A vaccine strain for an upcoming season may be identified as one which maximizes the joint probability of simultaneously arising from each (or most) of the currently circulating strains (Fig. 1c). This might not be a correct mechanistic picture per se (in which clades and their relative fitness might be more important⁶), but can still serve as a useful conceptualization if we are interested in estimating the vaccine strain, and not the full strain distribution. The vaccine strain identified in this manner does not deterministically specify a frequency-dominant strain, but a strain satisfying this criterion has high odds of being close to the distribution of circulating strains that emerge in the targeted future time-frame. Simplifying, we ultimately obtain the following search criteria (See derivation in “Predicting Seasonal Vaccine Strains” in Methods & Materials) to identify historical strain(s) that are expected to be maximally representative of the future distribution of circulation:

$$x_*^{t+\delta} = \arg \min_{y \in \cup_{\tau \leq t} H^\tau} \left(\sum_{x \in H^t} \theta_{m_t}(x, y) - |H^t| A \ln \omega_y \right) \quad (1)$$

where $x_*^{t+\delta}$ is a predicted vaccine strain at time $t + \delta$, H^t is the set of currently circulating human strains at time t observed over the past year, θ_{m_t} is the E-distance induced by Emergenet m_t inferred with sequences in H^t , ω_y is the persistence probability (See Def. 3 in Methods & Materials) of strain y in the inferred Emergenet which can be shown to be proportional to its replicative fitness (See “Relating Persistence Probability to Replicative Fitness” in Methods & Materials), and A is a constant dependent on the sequence length and significance threshold. Thus, we have a straightforward interpretation for Eq. (1): the first term requires the solution to be as close as possible to the centroid of the current strain distribution (in the E-distance metric), while the second term penalizes for low replicative fitness (See “Predicting Seasonal Vaccine Strains” in Methods & Materials). Eq. (1) does not attempt to replicate the future strain distribution, and thus is not claimed to be a mechanistically correct picture of the evolutionary process; but a computational criteria for identifying a vaccine strain candidate.

For validation of this scheme, we define the distance to the future circulation at time $t + \delta$ for sequence x as the average Hamming distance, h , between x and each sequence y in the future population $H^{t+\delta}$, weighted by its frequency $f_{t+\delta}(y)$, following recent evaluation approaches in the literature⁶. We predict one year into the future, $\delta = 1$, and thus:

$$d_\delta(x) = \sum_{y \in H^{t+\delta}} f_{t+\delta}(y) h(x, y) \quad (2)$$

In Eq. (1), we are making the assumption that H^t is a single cluster of strains. In practice, this might not be the case; we often see several distinct clusters arise in each season, which are functionally similar to the notion of clades⁶. Identifying clusters on the E-distance matrix $H_1^t, H_2^t, \dots, H_n^t$ with $\bigcup_{i=1}^n H_i^t = H^t$, we compute cluster-specific predictions $x_{i*}^{t+\delta}$ using Eq. (1), and obtain the unique vaccine recommendation as the weighted centroid of these cluster-specific recommendations, where the weights are the cluster sizes, *i.e.*:

$$x_*^{t+\delta} = \arg \min_{x \in \{x_{i*}^{t+\delta}\}} \sum_{i=1}^n h(x_{i*}^{t+\delta}, x) |H_i^t| \quad (3)$$

Using instantaneous clusters instead of standard clades allows for simplified calculations with no phylogenetic tree construction. This approach, which while possibly losing some information related to common ancestors, actually improves predictive performance. Also, we can make multiple predictions per season, *e.g.*, reporting the recommendations of the two largest clusters, as is shown in Fig. 2g-j, which dramatically improves predictive performance as expected.

Prediction of the seasonal vaccine strain as a close match to a historical strain allows out-of-sample validation against past World Health Organization (WHO) recommendations for the flu shot, which is reformulated February and September of each year for the northern and southern hemispheres, respectively, based on a cocktail of historical strains determined via global surveillance³⁴. For each year of the past two decades, we constructed a separate Emergenet for the southern and northern flu seasons using HA strains available from the previous season. For seasons with > 3000 strains available, we randomly sampled 3000 strains which provide an accurate representation of the population. We show in Supplementary Fig. S-5 that sampling has little effect on our results.

Our Emergenet-informed forecasts outperform WHO/CDC recommended flu vaccine compositions consistently over the past two decades, for both H1N1 and H3N2 subtypes, across both hemispheres (which have distinct recommendations⁷). Over the last two decades, the Emergenet H1N1 recommendations $x_*^{t+\delta}$ outperform WHO’s vaccine recommendations by, on average, 3.73 amino acids (AAs) in the north and 4.19 AAs in the south. For H3N2, this out-performance is 3.32 AAs in the north and 2.01 AAs in the south. Detailed predictions are tabulated in Extended Data Tables 1 through 5, including averages over the last decade. Visually, Fig. 2 illustrates the relative Emergenet improvement.

We also compare our performance with recently reported vaccine-strain prediction results⁶ at identical time points with better or comparable performance. Huddleston *et al.*’s model using mutational load and local branching index (LBI) outperforms the WHO vaccine by 1.93 AAs on average, while over the same time points, we outperform the WHO vaccine by 2.05 AAs. Our ability to obtain comparable performance with only sequence features demonstrates the added predictive information that the Emergenet is able to extract. The full comparison can be found in Extended Data table 6. While using Hemagglutinin inhibition (HI) antigenic novelty data Huddleston *et al.* outperforms the WHO vaccine by 2.33 AAs on average, this added information requires experimental evaluation of individual strains precluding scale-up and presenting challenges in generalizing to other viruses.

To evaluate a strategy of two-strain predictions, we evaluated two-cluster predictions $x_{1*}^{t+\delta}$ and $x_{2*}^{t+\delta}$ by taking the average minimum Hamming distance between $x_{1*}^{t+\delta}$ and $x_{2*}^{t+\delta}$ and the sequence population, we see a performance improvement. Over the last two decades, the two-cluster Emergenet H1N1 recommendations $x_*^{t+\delta}$ outperform WHO’s vaccine recommendations by 4.69 AAs in the north and 5.52 AAs in the south. For H3N2, this out-performance is 4.64 AAs in the north and 3.43 AAs in the south.

To confirm the robustness of our method, we also ask how our recommendations perform against selecting random strains. We select a random strains from each season to be our random “predictions”, choosing from strains circulating in the past one year leading up to vaccine selection, and compare them using our distance to the future metric (Eq. (2)). We repeat this for 20 random strains per season and report the mean. Over the last two decades, the Emergenet H1N1 recommendations $x_*^{t+\delta}$ outperform the random recommendations by 3.98 AAs (29.69%) in the north and 7.31 AAs (46.03%) in the south. For H3N2, this out-performance is 2.94 AAs (37.37%) in the north and 3.23 AAs (35.54%) in the

south (Extended Data Table 7). Over one decade the Emergenet out-performance is higher for H1N1 (> 70%), while for H3N2 it remains comparable (> 30%).

Comparing the Emergenet inferred strain (ENT) against the one recommended by the WHO, we find that the residues that only the Emergenet recommendation matches correctly with a common strain denoted as DOM (near dominant or strain observed with maximal frequency), while the WHO recommendation fails, are largely localized within the RBD, with > 57% occurring within the RBD on average (Extended Data Fig. 1a), and when the WHO strain deviates from the ENT/DOM matched residue, the “correct” residue is often replaced in the WHO recommendation with one that has very different side chain, hydrophathy and/or chemical properties (Extended Data Fig. 1b-f), suggesting deviations in recognition characteristics^{35,36}. Combined with the fact that we find circulating strains are almost always within a few edits of the DOM (Supplementary Fig. S-6), these observations suggest that hosts vaccinated with the ENT recommendation is can have season-specific antibodies that recognize a larger cross-section of the circulating strains.

Estimating Emergence Risk of Non-human Strains

Our primary claim is the ability to estimate the emergence potential of animal strains that do not yet circulate in humans. While modeling approaches for seasonal vaccine strain choice has been explored before, the problem of modeling emergence risk for animal strains is largely open. We propose a time-dependent Emergence Potential score E-risk $\rho_t(x)$ for an animal strain x in Eq. (4). Our risk measure is defined as the negative logarithm of the geometric mean of minimum E-distance to recent human HA and NA sequences, where the E-distance correspond to Emergenets constructed in a subtype specific manner from human sequences.

Before going into details, we need some more notation, which we keep consistent as much as possible with Eq. (1). For any strain y , we denote the HA and NA sequences as y^H, y^N respectively, and for a E-distance function induced for Emergenet r is denoted as $\theta_r(\cdot, \cdot)$. To validate our score against CDC-estimated IRAT emergence scores using E-risk, we constructed Emergenet models for HA and NA sequences using subtype-specific human strains, collected within the year prior to the assessment date, *e.g.*, the assessment date for A/swine/Shandong/1207/2016 is 06/2020, and we use all human strains collected between 01/07/2019 and 06/30/2020 for the Emergenet inference. More specifically, for each HA subtype for which sufficient number of sequences are collected in the span of one year leading up to that point (*e.g.* H1Nx, H3Nx, etc.), we construct a separate Emergenet model. The set of all Emergenet models so inferred for HA strains are denoted as \mathbb{E}^H , and all models for NA sequences are denoted as \mathbb{E}^N . With these notations, we define:

$$\rho_t(x) \triangleq -\log \min_{\substack{y, z \in H^t \\ r \in \mathbb{E}^H, s \in \mathbb{E}^N}} \sqrt{\theta_r(x^H, y^H) \theta_s(x^N, z^N)}, \text{ where } H^t \text{ defined as before in Eq. (1)} \quad (4)$$

We claim that larger the value of $\rho_t(x)$ larger the probability of jumping to a well-adapted human strain (See “Measure of Emergence Potential” in Methods & Materials). Strains observed to circulate in humans (*i.e.* those in H^t) are obviously well-adapted to humans, since we are only likely to sample common strains. Using Theorem 1 (See Methods & Materials):

$$\left| \ln \frac{Pr(x \rightarrow x_h)}{Pr(x_h \rightarrow x_h)} \right| \leq \beta \theta(x, x_h), \quad (5)$$

where x, x_h are respectively protein sequences (HA or NA) corresponding to an animal and a well-adapted human strain, and β is a constant. Importantly, when $\theta(x, x_h)$ is close to zero and $Pr(x_h \rightarrow x_h)$ is large, it follows that $Pr(x \rightarrow x_h)$ is large as well, justifying the claim (See “Measure of Emergence Potential” in Methods & Materials). Thus, in both vaccine strain prediction and emergence risk estimation, our approach is predicated on our inferred models to correctly relate E-distance $\theta(x, y)$ to the probability $Pr(x \rightarrow y)$, and hence good performance on the first problem gives confidence about the results in the second. The geometric mean ensures equal weighting of both HA and NA (this is the simplest assumption), and the logarithm in Eq. (4) ensures that scale of our measure matches with that of CDC-estimated IRAT scores, and this comparison provides quantitative validation of our framework.

Our approach ensures that, we can obtain a E-risk score for animal sequences that do not have any human sequences of the same subtype. For example, \mathbb{E}^H comprises Emergenet models for H1, H3, H5, H7, and \mathbb{E}^N comprises models for N1, N2, N9 (for some years H5 Emergenet is not constructed due to not enough sequences found in the previous one year). Now suppose we observe a (yet non existent) animal strain H14N12. We will carry out the minimizations stated in Eq. (4) with the HA sequence of this strain considering all human HA sequences observed in the past year using each of the HA Emergenets in \mathbb{E}^H , and with the NA sequence of this strain again against all human NA sequences of strains observed within the past year using each of the NA Emergenets in \mathbb{E}^N : it does not matter that we do not have a Emergenet for H14N12, or that this strain is yet to be observed in humans.

Considering IRAT emergence scores of 23 strains published by the CDC, we find strong out-of-sample support (total least squares correlation: 0.721, p-value: 0.00010, Fig. 3) for this claim. We also fit total least squares models against IRAT’s “Mean Low Acceptable Emergence”, a lower bound on the estimate of the emergence score (correlation: 0.685, p-value: 0.00061) and “Mean High Acceptable Emergence”, an upper bound (correlation: 0.733, p-value: 0.00016). We take approximately 30 seconds (on a 28-core Intel processor) as opposed to potentially weeks taken by IRAT experimental assays and SME evaluation. Full results can be found in Extended Data Table 8.

Note that the nature of risk implies that a “high-risk” strain is not guaranteed to emerge, and neither IRAT nor our

assessment should be dismissed on the basis that a high-risk strain did not cause a pandemic. However, to interpret our high correlative association with the CDC-computed IRAT scores as validation of our claim, there needs to be some evidence that the IRAT scores themselves are good predictors of emergence. In addition to the CDC's expert-consensus driven methodology being the best alternative to direct gold-standard checks (which are impossible for ethical and legal reasons), we also have evidence that some high-risk strains did corroborate with emergence events (Supplementary Table S-4), including A/swine/Shandong/1207/2016, A/Ohio/13/2017, A/Hong Kong/125/2017, and A/California/62/2018; the last one was indeed isolated in human hosts³⁷.

Since biosurveillance is expected to be only sparsely sampling the wild reservoirs, we investigated how limited and incomplete sampling of the animal strain distribution impacts our estimated emergence scores (Extended Data Table 10), to quantify uncertainty in the estimates. Instead of using all available human strains, we chose a random sample of 75% of the available human strains of the appropriate sub-types to construct the Emergenet models, and used the same sample to compute the emergence scores. As shown in the Extended Data Table 10, the SEM of the score estimates are at least an order of magnitude smaller than the estimates themselves, suggesting that the scores stabilize for a reasonable sampling of the wild distributions.

A second demonstration of our approach is obtained by computing the E-risk scores for "variants" (animal Influenza A strains isolated in human hosts), which might be expected to pose high risk due to their successful replication in human cells, even if the possibility of HH transmission is not yet observed or guaranteed. We analyze 15 such variants isolated post-2015 listed as antigenic prototypes for candidate vaccine viruses by the CDC³⁸ (Supplementary Table S-5). Our E-risk estimates puts approximately 30% of these variants in the high risk category (the 5% tail of the distribution of emergence scores amongst all animal strains collected post 2020, Supplementary Fig. S-7-a). More specifically (Supplementary Table S-6), we note that 26.7% of the variants have emergence score > 7.0 compared to 6.4% of the strains in the animal reservoirs, suggesting, as expected, the variants pose much higher risk. Indeed 4 out of the 15 variants have scores greater than 7.0. Additionally, we see in Supplementary Fig. S-8, that the risk posed by the high-risk variants can be seen to be generally increasing over time, up to the point of collection in human hosts.

Finally, we estimate the IRAT scores of all 6,354 wild Influenza A animal viruses collected globally between January 2020 and January 2024. We trained HA and NA Emergenet models for each subtype using recent sequence data, computed E-risk using the same method as described above, and identified the ones posing maximal risk (Fig. 3c). 413 strains turn out to have a predicted emergence score > 7 (top 15th percentile, and the 95% significance threshold for a normal distribution fit, Supplementary Fig. S-7-a), and 190 strains have score > 7.3 (top 10th percentile). However, many of these strains are highly similar, differing by only a few edits. To identify the sufficiently distinct risky strains, we constructed the standard phylogeny from HA sequences with score > 6.25 (Fig. 4), and collapsed all leaves within 15 edits, showing only the most risky strain within a collapsed group. This leaves 80 strains (Fig. 4), with 12 having emergence risk > 7 , and 10 with risk above 7.3 (top 10 rows in Extended Data Table 12, see also the distribution of the scores of this set in Supplementary Fig. S-7-b). Subtypes of the risky strains are H7N9(1), H1N2(2), H3N2(2), H1N1(2) and H5N1(3) with the top 5 most risky strains as follows: A/Hong Kong/125/2017(H7N9), A/California/62/2018(H1N2), A/swine/Missouri/A02524408/2023(H3N2), A/swine/Tver_region/R11-81-1S/2023(H1N1), A/swine/North_Carolina/A02479173/2020(H1N1), A/Common_Buzzard/England/125155/2023(H5N1).

To visually check if high risk strains are edit-wise closer to human strains, we compare the HA sequences along with two frequency dominant human strains in 2021-2022 season (Extended Data Fig. 2,1,2 and 3). High-risk strains are somewhat closer in number of edits to these high frequency human strains, but both cases (high and low risk) show substantial residue replacements, both in and out of the receptor binding domain (RBD), to make reliable assessments unreliable without the use of the E-risk score.

Broadly the risk assessments are not surprising: swines are known to be efficient mixing vessels^{3,39-41}, and hence unsurprisingly host a large fraction of the risky strains ($> 63\%$ over 7.0). A large diversity of avian hosts for the strains ($> 30\%$ over 7.0, $> 70\%$ of the reduced set with score > 6.25) explains our finding of large number of high risk H5N1 strains (avian flu) among the high-risk set, which correlates with current increasing concerns about H5N1⁴², with at least two reported human cases in May 2024. Thus, qualitatively our results are well aligned with the current expectations; nevertheless the ability to quantitatively rank specific strains which pose maximal risk is a crucial new capability enabling proactive pandemic mitigation efforts.

Conclusion

While numerous tools exist for ad hoc quantification of genomic similarity^{9,18,43-46}, higher similarity between strains in these frameworks is not sufficient to imply a high likelihood of a jump. To the best of our knowledge, the Emergenet algorithm is the first of its kind to learn an appropriate biologically meaningful comparison metric from data, without assuming any model of DNA or amino acid substitution, or a genealogical tree a priori. While the effect of the environment and selection cannot be inferred from a single sequence, an entire database of observed strains, processed through the right lens, can parse out useful predictive models of these complex interactions. Our results are aligned with recent studies demonstrating effective predictability of future mutations for different organisms^{47,48}.

The E-distance calculation is currently limited to analogous sequences (such as point variations of the same protein from different viral subtypes), and the Emergenet inference requires a sufficient diversity of observed strains. A multi-

variate regression analysis indicates that the most important factor for our approach to succeed is the diversity of the sequence dataset (See “Multivariate Regression to Understand Data Characteristics Necessary For Emergent Modeling” in Methods & Materials and Supplementary Table S-7), which would exclude applicability to completely novel pathogens with no related human variants, and ones that evolve very slowly. Nevertheless, the tools reported here can potentially improve effectiveness of the annual flu shot, and, more importantly, allow for the development of preemptive vaccines to target risky animal strains before the first human infection in the next pandemic. Apart from outlining new precision public health measures to avert pandemics, such strategies might also help to non-controversially counter the impact of vaccine hesitancy which has interfered with optimal pandemic response in recent times.

Data Source

We use two public sequence databases: 1) National Center for Biotechnology Information (NCBI) virus⁵⁵ and 2) GISAID⁵⁶ databases. The former is a community portal for viral sequence data, aiming to increase the usability of data archived in various NCBI repositories. GISAID has a more restricted user agreement, and use of GISAID data in an analysis requires acknowledgment of the contributions of both the submitting and the originating laboratories (Corresponding acknowledgment tables are included as supplementary information). We collected a total of 463,266 sequences in our analysis (see Supplementary Table S-1).

Data and Software Sharing

Working open-source software (requiring Python 3.x) is publicly available at <https://pypi.org/project/emergenet/>. All inferred Emergenet models inferred is available at <https://doi.org/10.5281/zenodo.7387861>.

REFERENCES

- [1] Shao, W., Li, X., Goraya, M. U., Wang, S. & Chen, J.-L. Evolution of influenza a virus by mutation and reassortment. *International journal of molecular sciences* **18**, 1650 (2017).
- [2] Mills, C. E., Robins, J. M. & Lipsitch, M. Transmissibility of 1918 pandemic influenza. *Nature* **432**, 904–906 (2004).
- [3] Reid, A. H. & Taubenberger, J. K. The origin of the 1918 pandemic influenza virus: a continuing enigma. *Journal of general virology* **84**, 2285–2292 (2003).
- [4] Landolt, G. A. & Olsen, C. W. Up to new tricks—a review of cross-species transmission of influenza a viruses. *Animal Health Research Reviews* **8**, 1–21 (2007).
- [5] Dos Santos, G., Neumeier, E. & Bekkat-Berkani, R. Influenza: Can we cope better with the unpredictable? *Human vaccines & immunotherapeutics* **12**, 699–708 (2016).
- [6] Huddleston, J. *et al.* Integrating genotypes and phenotypes improves long-term forecasts of seasonal influenza a/h3n2 evolution. *Elife* **9**, e60067 (2020).
- [7] Boni, M. F. Vaccination and antigenic drift in influenza. *Vaccine* **26**, C8–C14 (2008).
- [8] Tricco, A. C. *et al.* Comparing influenza vaccine efficacy against mismatched and matched strains: a systematic review and meta-analysis. *BMC medicine* **11**, 153 (2013).
- [9] Neher, R. A., Russell, C. A. & Shraiman, B. I. Predicting evolution from the shape of genealogical trees. *Elife* **3**, e03568 (2014).
- [10] Vergara-Alert, J. *et al.* The ns segment of h5n1 avian influenza viruses (aiv) enhances the virulence of an h7n1 aiv in chickens. *Veterinary research* **45**, 1–11 (2014).
- [11] Hothorn, T., Hornik, K. & Zeileis, A. Unbiased recursive partitioning: A conditional inference framework. *JOURNAL OF COMPUTATIONAL AND GRAPHICAL STATISTICS* **15**, 651–674 (2006).
- [12] Wille, M., Geoghegan, J. L. & Holmes, E. C. How accurately can we assess zoonotic risk? *PLoS biology* **19**, e3001135 (2021).
- [13] Pulliam, J. R. & Dushoff, J. Ability to replicate in the cytoplasm predicts zoonotic transmission of livestock viruses. *The Journal of infectious diseases* **199**, 565–568 (2009).
- [14] Grewelle, R. E. Larger viral genome size facilitates emergence of zoonotic diseases. *bioRxiv* (2020).
- [15] Grange, Z. L. *et al.* Ranking the risk of animal-to-human spillover for newly discovered viruses. *Proceedings of the National Academy of Sciences* **118**, e2002324118 (2021).
- [16] CDC. Influenza risk assessment tool (irat). <https://www.cdc.gov/flu/pandemic-resources/national-strategy/risk-assessment.htm> (2020). (Accessed on 02/20/2024).
- [17] Gamblin, S. J. & Skehel, J. J. Influenza hemagglutinin and neuraminidase membrane glycoproteins. *Journal of Biological Chemistry* **285**, 28403–28409 (2010).
- [18] Posada, D. & Crandall, K. A. Modeltest: testing the model of dna substitution. *Bioinformatics (Oxford, England)* **14**, 817–818 (1998).
- [19] Eng, C. L., Tong, J. C. & Tan, T. W. Predicting host tropism of influenza a virus proteins using random forest. *BMC medical genomics* **7**, 1–11 (2014).
- [20] Ahlquist, P. Rna-dependent rna polymerases, viruses, and rna silencing. *Science* **296**, 1270–1273 (2002).
- [21] Chen, R. & Holmes, E. C. Avian influenza virus exhibits rapid evolutionary dynamics. *Molecular biology and evolution* **23**, 2336–2341 (2006).

- [22] Woolthuis, R. G., van Dorp, C. H., Keşmir, C., de Boer, R. J. & van Boven, M. Long-term adaptation of the influenza a virus by escaping cytotoxic t-cell recognition. *Scientific reports* **6**, 1–8 (2016).
- [23] Fan, K. *et al.* Role of itk signalling in the interaction between influenza a virus and t-cells. *Journal of general virology* **93**, 987–997 (2012).
- [24] van de Sandt, C. E. *et al.* Differential recognition of influenza a viruses by m158–66 epitope-specific cd8+ t cells is determined by extraepitopic amino acid residues. *Journal of virology* **90**, 1009–1022 (2016).
- [25] Berkhoff, E., Geelhoed-Mieras, M., Fouchier, R., Osterhaus, A. & Rimmelzwaan, G. Assessment of the extent of variation in influenza a virus cytotoxic t-lymphocyte epitopes by using virus-specific cd8+ t-cell clones. *Journal of General Virology* **88**, 530–535 (2007).
- [26] Van de Sandt, C. E., Kreijtz, J. H. & Rimmelzwaan, G. F. Evasion of influenza a viruses from innate and adaptive immune responses. *Viruses* **4**, 1438–1476 (2012).
- [27] Wood, J. M. *et al.* Reproducibility of serology assays for pandemic influenza h1n1: collaborative study to evaluate a candidate who international standard. *Vaccine* **30**, 210–217 (2012).
- [28] Cover, T. M. & Thomas, J. A. *Elements of Information Theory (Wiley Series in Telecommunications and Signal Processing)* (Wiley-Interscience, New York, NY, USA, 2006).
- [29] Caton, A., Brownlee, G., Yewdell, J. & Gerhard, W. The antigenic structure of the influenza virus a/pr/8/34 hemagglutinin (h1 subtype). *Cell* **31**, 417–427 (1982).
- [30] Koelle, K., Cobey, S., Grenfell, B. & Pascual, M. Epochal evolution shapes the phylodynamics of interpandemic influenza a (h3n2) in humans. *Science* **314**, 1898–1903 (2006).
- [31] Lou, Y., Caruana, R. & Gehrke, J. Intelligible models for classification and regression. In *Proceedings of the 18th ACM SIGKDD International Conference on Knowledge Discovery and Data Mining*, 150–158 (Association for Computing Machinery, New York, NY, USA, 2012).
- [32] Lundberg, S. M. & Lee, S.-I. A unified approach to interpreting model predictions. In *Advances in neural information processing systems*, vol. 30, 4765–4774 (2017).
- [33] Shapley, L. S. A value for n-person games. In *Contributions to the Theory of Games*, vol. 2, 307–317 (Princeton University Press, 1953).
- [34] Agor, J. K. & Özalpın, O. Y. Models for predicting the evolution of influenza to inform vaccine strain selection. *Human vaccines & immunotherapeutics* **14**, 678–683 (2018).
- [35] Carugo, O. & Pongor, S. A normalized root-mean-square distance for comparing protein three-dimensional structures. *Protein science* **10**, 1470–1473 (2001).
- [36] Righetto, I., Milani, A., Cattoli, G. & Filippini, F. Comparative structural analysis of haemagglutinin proteins from type a influenza viruses: conserved and variable features. *BMC bioinformatics* **15**, 363 (2014).
- [37] of Public Health, C. D. Annual immunization report 2017-2018 (2018). URL <https://www.cdph.ca.gov/Programs/CID/DCDC/CDPH%20Document%20Library/Immunization/Annual2017-18.pdf>. Accessed: 2024-05-31.
- [38] World Health Organization. Summary of influenza a (h1) candidate vaccine viruses for pandemic preparedness (2023). URL https://cdn.who.int/media/docs/default-source/influenza/cvvs/cvv-zoonotic---southern-hemisphere-2023/summary_a_h1v_cvv_20220928.pdf?sfvrsn=c9567a3c_5. Accessed: 2024-05-30.
- [39] Ma, W., Kahn, R. E. & Richt, J. A. The pig as a mixing vessel for influenza viruses: human and veterinary implications. *Journal of molecular and genetic medicine: an international journal of biomedical research* **3**, 158 (2009).
- [40] Nelson, M. I. & Worobey, M. Origins of the 1918 pandemic: revisiting the swine “mixing vessel” hypothesis. *American journal of epidemiology* **187**, 2498–2502 (2018).
- [41] Baumann, J., Kouassi, N. M., Foni, E., Klenk, H.-D. & Matrosovich, M. H1N1 Swine Influenza Viruses Differ from Avian Precursors by a Higher pH Optimum of Membrane Fusion. *Journal of virology* (2015).
- [42] for Disease Control, C. & Prevention. Cdc reports human case of h5n1 (2024). URL <https://www.cdc.gov/media/releases/2024/s0522-human-case-h5.html>. Accessed: 2024-05-25.
- [43] Goldberger, A. L. & Peng, C.-K. Genomic classification using an information-based similarity index: application to the sars coronavirus. *Journal of Computational Biology* **12**, 1103–1116 (2005).
- [44] Huelsenbeck, J. P. & Crandall, K. A. Phylogeny estimation and hypothesis testing using maximum likelihood. *Annual Review of Ecology and systematics* **28**, 437–466 (1997).
- [45] van der Meer, F. J. U. M., Orsel, K. & Barkema, H. W. The new influenza A H1N1 virus: balancing on the interface of humans and animals. *The Canadian veterinary journal = La revue veterinaire canadienne* **51**, 56–62 (2010).
- [46] Smith, G. J. D. *et al.* Origins and evolutionary genomics of the 2009 swine-origin H1N1 influenza A epidemic. *Nature* **459**, 1122–1125 (2009).
- [47] Mollentze, N., Babayan, S. A. & Streicker, D. G. Identifying and prioritizing potential human-infecting viruses from their genome sequences. *PLoS biology* **19**, e3001390 (2021).
- [48] Maher, M. C. *et al.* Predicting the mutational drivers of future sars-cov-2 variants of concern. *Science Translational Medicine* **14**, eabk3445 (2022).
- [49] Hernández-Orozco, S., Kiani, N. A. & Zenil, H. Algorithmically probable mutations reproduce aspects of evolution, such as convergence rate, genetic memory and modularity. *Royal Society open science* **5**, 180399 (2018).
- [50] Vanmarcke, E. *Random fields: analysis and synthesis* (World scientific, 2010).
- [51] Manning, C. D., Manning, C. D. & Schütze, H. *Foundations of statistical natural language processing* (MIT press, 1999).

-
- [52] Varadhan, S. S. Large deviations. In *Proceedings of the International Congress of Mathematicians 2010 (ICM 2010) (In 4 Volumes) Vol. I: Plenary Lectures and Ceremonies Vols. II–IV: Invited Lectures*, 622–639 (World Scientific, 2010).
- [53] Carreira-Perpinán, M. A. A review of mean-shift algorithms for clustering. *arXiv preprint arXiv:1503.00687* (2015).
- [54] Fedotov, A. A., Harremoës, P. & Topsøe, F. Refinements of pinsker's inequality. *IEEE Transactions on Information Theory* **49**, 1491–1498 (2003).
- [55] Hatcher, E. L. *et al.* Virus variation resource–improved response to emergent viral outbreaks. *Nucleic acids research* **45**, D482–D490 (2017).
- [56] Bogner, P., Capua, I., Lipman, D. J. & Cox, N. J. A global initiative on sharing avian flu data. *Nature* **442**, 981–981 (2006).
- [57] Wu, N. C. & Wilson, I. A. Influenza hemagglutinin structures and antibody recognition. *Cold Spring Harbor perspectives in medicine* **10**, a038778 (2020).
- [58] Tzarum, N. *et al.* Structure and receptor binding of the hemagglutinin from a human h6n1 influenza virus. *Cell host & microbe* **17**, 369–376 (2015).
- [59] Lazniewski, M., Dawson, W. K., Szczepińska, T. & Plewczynski, D. The structural variability of the influenza a hemagglutinin receptor-binding site. *Briefings in functional genomics* **17**, 415–427 (2018).
- [60] Garcia, N. K., Guttman, M., Ebner, J. L. & Lee, K. K. Dynamic changes during acid-induced activation of influenza hemagglutinin. *Structure* **23**, 665–676 (2015).
- [61] Yin, J. *et al.* Effects of ambient temperature on influenza-like illness: A multicity analysis in shandong province, china, 2014–2017. *Frontiers in Public Health* **10** (2023). URL <https://www.frontiersin.org/articles/10.3389/fpubh.2022.1095436>.
- [62] Sun, H. *et al.* Prevalent eurasian avian-like h1n1 swine influenza virus with 2009 pandemic viral genes facilitating human infection. *Proceedings of the National Academy of Sciences* **117**, 17204–17210 (2020). URL <https://www.pnas.org/doi/abs/10.1073/pnas.1921186117>. <https://www.pnas.org/doi/pdf/10.1073/pnas.1921186117>.
- [63] CDC. Estimated flu-related illnesses, medical visits, hospitalizations, and deaths in the united states — 2017–2018 flu season. <https://www.cdc.gov/flu/about/burden/2017-2018.htm> (2021). (Accessed on 06/25/2023).
- [64] Kile, J. C. *et al.* Update: Increase in human infections with novel asian lineage avian influenza a(h7n9) viruses during the fifth epidemic — china, october 1, 2016–august 7, 2017. <http://dx.doi.org/10.15585/mmwr.mm6635a2> (2017).

ACKNOWLEDGMENTS

This work has been partly funded by the PREEMPT program from Defense Advanced Research Projects Agency (D19AC00004/N/A), and intramural grants from the University of Chicago, Biological Science Division.

Supplementary Materials

METHODS & MATERIALS

We briefly describe the proposed computational framework.

Emergenet Framework

We do not assume that the mutational variations at the individual indices of a genomic sequence are independent (See Fig 1a). Irrespective of whether mutations are truly random⁴⁹, since only certain combinations of individual mutations are viable, individual mutations across a genomic sequence replicating in the wild appear constrained, which is what is explicitly modeled in our approach.

Consider a set of random variables $X = \{X_i\}$, with $i \in \{1, \dots, N\}$, each taking value from the respective sets Σ_i . Here each X_i is the random variable modeling the “outcome” *i.e.* the AA residue at the i^{th} index of the protein sequence. A sample $x \in \prod_1^N \Sigma_i$ is an ordered N -tuple, which is a specific strain in this context, consisting of a realization of each of the variables X_i with the i^{th} entry x_i being the realization of random variable X_i .

We use the notation x_{-i} and $x^{i,\sigma}$ to denote:

$$x_{-i} \triangleq x_1, \dots, x_{i-1}, x_{i+1}, \dots, x_N \quad (6a)$$

$$x^{i,\sigma} \triangleq x_1, \dots, x_{i-1}, \sigma, x_{i+1}, \dots, x_N, \sigma \in \Sigma_i \quad (6b)$$

Also, $\mathcal{D}(S)$ denotes the set of probability measures on a set S , *e.g.*, $\mathcal{D}(\Sigma_i)$ is the set of distributions on Σ_i .

We note that X defines a random field⁵⁰ over the index set $\{1, \dots, N\}$.

Definition 1 (Emergenet). *For a random field $X = \{X_i\}$ indexed by $i \in \{1, \dots, N\}$, the Emergenet is defined to be the set of predictors $\Phi = \{\Phi_i\}$, *i.e.*, we have:*

$$\Phi_i : \prod_{j \neq i} \Sigma_j \rightarrow \mathcal{D}(\Sigma_i), \quad (7)$$

where for a sequence x , $\Phi_i(x_{-i})$ estimates the distribution of X_i on the set Σ_i .

We use conditional inference trees as models for predictors¹¹, although more general models are possible.

Biology-Aware Distance Between Sequences

The mathematical form of our metric is not arbitrary; JS divergence is a symmetricised version of the more common KL divergence²⁸ between distributions, and among different possibilities, the E-distance is the simplest metric such that the likelihood of a spontaneous jump (See Eq. (10) in Methods) is provably bounded above and below by simple exponential functions of the E-distance.

Definition 2 (E-distance: adaptive biologically meaningful dissimilarity between sequences). *Given two sequences $x, y \in \prod_1^N \Sigma_i$, such that x, y are drawn from the populations P, Q inducing the Emergenet Φ^P, Φ^Q , respectively, we define a pseudo-metric $\theta(x, y)$, as follows:*

$$\theta(x, y) \triangleq \mathbf{E}_i \left(\mathbb{J}^{\frac{1}{2}} \left(\Phi_i^P(x_{-i}), \Phi_i^Q(y_{-i}) \right) \right) \quad (8)$$

where $\mathbb{J}(\cdot, \cdot)$ is the Jensen-Shannon divergence⁵¹ and \mathbf{E}_i indicates expectation over the indices.

The square-root in the definition arises naturally from the bounds we are able to prove, and is dictated by the form of Pinsker's inequality²⁸, ensuring that the sum of the length of successive path fragments equates the length of the path.

Persistence Probability

We can formulate a computable characteristic for a sequence x that is related to the more popular notion of replicative fitness. Referred to as *persistence probability* of the sequence x , we note that the probability $Pr(x \rightarrow x)$ is the probability that a sequence does not “jump away”, and higher these odds, lower are the odds that there are incentives to change, *i.e.*, higher the replicative fitness.

Definition 3 (Persistence probability of a sequence). *Given a population P inducing the Emergenet Φ^P and a sequence x , we can estimate the probability $Pr(x \rightarrow x)$, denoted as the persistence probability of x as:*

$$\omega_x^P \triangleq Pr(x \rightarrow x) = \prod_{j=1}^N (\Phi_j^P(x_{-j})|_{x_j}) \quad (9)$$

x_j is the j^{th} entry in x , and is thus an element in the set Σ_j . Since we are mostly concerned with the case where Σ_j is a finite set, $\Phi_j^P(x_{-j})|_{x_j}$ is the entry in the probability mass function corresponding to the element of Σ_j which appears at the j^{th} index in sequence x .

Relating Persistence Probability to Replicative Fitness

The concept of replicative fitness, denoted as $f(x)$, is fundamentally connected to the persistence probability of a strain, ω_x , which as per the definition above, is the likelihood that a strain x reproduces into itself rather than mutating into a different strain. Mathematically, this relationship can be derived by considering the population dynamics of strain x . The change in the population $N_x(t)$ of strain x over time can be modeled as:

$$\frac{dN_x(t)}{dt} = f(x)N_x(t) - \mu_x N_x(t),$$

where $f(x)$ is the replicative fitness of strain x and μ_x is the mutation rate to other strains. This equation indicates that the net growth rate of the population is determined by the difference between the replication rate and the mutation rate:

$$\frac{dN_x(t)}{dt} = (f(x) - \mu_x)N_x(t).$$

To express the persistence probability ω_x of strain x , we consider the probability that the strain reproduces into itself rather than mutating. This can be formulated as the ratio of the replication rate to the total rate of change, which includes both replication and mutation:

$$\omega_x = \frac{f(x)}{f(x) + \mu_x}.$$

thus that the persistence probability is directly proportional to the replicative fitness and inversely proportional to the mutation rate. Higher replicative fitness $f(x)$ leads to a higher persistence probability ω_x , while higher mutation rates μ_x reduce the persistence probability. Therefore, strains with higher fitness are more likely to maintain their genetic identity over time, ensuring their continued presence in the population. This relationship underscores the critical role of replicative fitness in the evolutionary success and stability of strains within a dynamic environment.

Theoretical Probability Bounds

The Emergenet framework allows us to rigorously compute bounds on the probability of a spontaneous change of one strain to another, brought about by chance mutations. While any sequence of mutations is equally likely, the ‘‘fitness’’ of the resultant strain, or the probability that it will even result in a viable strain, or not. Thus the necessity of preserving function dictates that not all random changes are viable, and the probability of observing some trajectories through the sequence space are far greater than others. The Emergenet framework allows us to explore this constrained dynamics, as revealed by a sufficiently large set of genomic sequences.

The mathematical intuition relating E-distance to the log-likelihood of spontaneous change is similar to quantifying the odds of a rare biased outcome when we toss a fair coin. While for an unbiased coin, the odds of roughly 50% heads is overwhelmingly likely, large deviations do happen rarely, and it turns out that the probability of such rare deviations can be explicitly quantified with existing statistical theory⁵². Generalizing to non-uniform conditional distributions inferred by the Emergenet, the likelihood of a spontaneous transition by random chance may also be similarly bounded.

We show in Theorem 1 in the supplementary text that at a significance level α , with a sequence length N , the probability of spontaneous jump of sequence x from population P to sequence y in population Q , $Pr(x \rightarrow y)$, is bounded by:

$$\omega_y^Q e^{\frac{\sqrt{8}N^2}{1-\alpha}\theta(x,y)} \geq Pr(x \rightarrow y) \geq \omega_y^Q e^{-\frac{\sqrt{8}N^2}{1-\alpha}\theta(x,y)} \quad (10)$$

where ω_y^Q is the persistence probability of strain y in the target population, N is the sequence length, and α is the statistical significance level.

Predicting Seasonal Vaccine Strains

Analyzing the distribution of sequences observed to circulate in the human population at the present time allows us to forecast effective vaccine strain(s) in the next flu season as follows:

Let $x_*^{t+\delta}$ be a strain that will be in circulation in the upcoming flu season at time $t + \delta$, where H^t is the set of observed strains presently in circulation in the human population (at time t). We will assume that the Emergenet is constructed using the sequences in the set H^t , and remains unchanged upto $t + \delta$. Since this set is a function of time, the inferred Emergenet also changes with time, and the induced E-distance is denoted as $\theta^{[t]}(\cdot, \cdot)$.

Let us estimate $x_*^{t+\delta}$ as the strain that has the maximum average probability of arising from the current strain distribution. From the RHS bound established in Theorem 1 (See Eq. (10) above) in the supplementary text, we have for a strain $x \in H^t$:

$$\ln \frac{Pr(x \rightarrow x_*^{t+\delta})}{\omega_{x_*^{t+\delta}}} \geq -\frac{\sqrt{8}N^2}{1-\alpha}\theta^{[t]}(x, x_*^{t+\delta}) \quad (11)$$

$$\Rightarrow \sum_{x \in H^t} \ln \frac{Pr(x \rightarrow x^{t+\delta})}{\omega_{x^{t+\delta}}} \geq \sum_{x \in H^t} -\frac{\sqrt{8}N^2}{1-\alpha} \theta^{[t]}(x, x^{t+\delta}) \quad (12)$$

$$\Rightarrow \sum_{x \in H^t} \theta^{[t]}(x, x^{t+\delta}) - |H^t| A \ln \omega_{x^{t+\delta}} \geq A \ln \frac{1}{\prod_{x \in H^t} Pr(x \rightarrow x^{t+\delta})} \quad (13)$$

where $A = \frac{1-\alpha}{\sqrt{8}N^2}$, where N is the sequence length considered, and α is a fixed significance level. Since **minimizing the LHS maximizes the lower bound on the probability of the observed strains simultaneously giving rise to $x^{t+\delta}$** , $x_*^{t+\delta}$ may be estimated as a solution to the optimization problem:

$$x_*^{t+\delta} = \arg \min_{y \in \cup_{\tau \leq t} H^\tau} \left(\sum_{x \in H^t} \theta^{[t]}(x, y) - |H^t| A \ln \omega_y \right) \quad (\text{Eq. (1)})$$

We can explicitly interpret the two terms in the Eqn. 1. The first term clearly minimizes the distance from the centroid, measured in the E-distance metric. This alone will suffice in a static population, and has been observed before using the edit distance metric⁶. The second term penalizes the solution if it has lower replicative fitness. This justifies the interpretation that Eqn. 1 prescribes the optimal solution as one that is close to the centroid of the circulating strain in recent past, while penalizing strains which do not have high replicative fitness. While this explanation probably seems obvious after the fact, the above argument derives it precisely, and highlights the role of the Emergenet.

For validation of this scheme, we define the distance to the future circulation at time $t + \delta$ for sequence x as the average Hamming distance, h , between x and each sequence y in the future population $H^{t+\delta}$, weighted by its frequency $f_{t+\delta}(y)$, following recent evaluation approaches in the literature⁶. We predict one year into the future, $\delta = 1$, and thus:

$$d_\delta(x) = \sum_{y \in H^{t+\delta}} f_{t+\delta}(y) h(x, y) \quad (\text{Eq. (2)})$$

In Eq. (1), we are making the assumption that H^t is a single cluster of strains. In practice, this might not be the case; we often see several distinct clusters arise in each season, which are often aligned with the distinct clades. We can cluster the strains using a clustering method (here we use the MeanShift algorithm⁵³) on the E-distance matrix computed between strains in H^t such that we have n disjoint clusters $H_1^t, H_2^t, \dots, H_n^t$ with $\bigcup_{i=1}^n H_i^t = H^t$. We then compute cluster-specific predictions $x_{i*}^{t+\delta}$ using Eq. (1), and obtain the unique vaccine recommendation as the weighted centroid of these cluster-specific recommendations, where the weights are the cluster sizes, *i.e.*:

$$x_*^{t+\delta} = \arg \min_{x \in \{x_{i*}^{t+\delta}\}_i} \sum_i h(x_{i*}^{t+\delta}, x) |H_i^t| \quad (14)$$

For two-cluster predictions where we aim to make two strain recommendations instead of one, we take the predictions $x_{1*}^{t+\delta}$ and $x_{2*}^{t+\delta}$ from the two largest clusters, H_1^t and H_2^t . Thus, we can make multiple predictions per season, by replacing H^t in Eq. (1) with H_i^t for $i = 1, 2, \dots, n$. When we provide recommendations for two vaccine strains, we take the predictions from the largest two clusters, as is shown in Fig. 2g-j in the main text.

Measure of Emergence Potential

Recall, Eq. (4) states our proposed measure for emergence potential for a strain x , which is negative logarithm of the geometric mean of minimum E-distance to recent human HA and NA sequences, where the E-distance correspond to Emergenets constructed in a subtype specific manner from human sequences. The key rationale can be established by considering only one protein (say HA), and only one subtype of human models, as follows.

Theorem 1 can be rewritten as such: for a strain x in animals, and a human circulating strain x_h , we have:

$$\left| \ln \frac{Pr(x \rightarrow x_h)}{Pr(x_h \rightarrow x_h)} \right| \leq \beta \theta(x, x_h), \text{ with } \beta = \frac{\sqrt{8}N^2}{1-\alpha} \quad (15)$$

Now assume that the human strain x_h is well-adapted to humans, implying that it has high fitness. A high fitness of any strain y may be interpreted as a high value for $Pr(y \rightarrow y)$, and in the extreme case $Pr(y \rightarrow y) \approx 1$. Now if the RHS of the above relationship is close to zero, we conclude:

$$\theta(x, x_h) \rightarrow 0 \Rightarrow Pr(x \rightarrow x_h) \rightarrow Pr(x_h \rightarrow x_h) \quad (16)$$

and

$$\theta(x, x_h) = 0 \Rightarrow Pr(x \rightarrow x_h) = Pr(x_h \rightarrow x_h) \quad (17)$$

This implies that for an animal strain x , a small E-distance to some well-adapted circulating human strain x_h implies a high jump probability to a similarly well-adapted human strain. Given a sufficiently large sample of well-adapted human strains, we can now quantify a measure of emergence potential as:

$$\rho_t(x) \triangleq -\log \min_{y \in H^t} \theta^{[t]}(x, y) \quad (18)$$

where as before H^t is the set of observed strains presently in circulation in the human population (at time t), restricted to observations over the past year. We do not use historical human strains from further back in time to prevent introducing errors from changing host immune characteristics over time.

A large value of the emergence potential defined above thus can be interpreted as a large probability of jumping to a

currently well-adapted human strain wrt to both HA and NA sequences, due to the geometric mean of E-distance wrt to HA and NA in Eq. (4).

Proof of Probability Bounds

Theorem 1 (Probability bound). *Given a sequence x of length N that transitions to a strain $y \in Q$, we have the following bounds at significance level α .*

$$\omega_y^Q e^{\frac{\sqrt{8}N^2}{1-\alpha}\theta(x,y)} \geq Pr(x \rightarrow y) \geq \omega_y^Q e^{-\frac{\sqrt{8}N^2}{1-\alpha}\theta(x,y)} \quad (19)$$

where ω_y^Q is the persistence probability of strain y in the target population Q (See Def. 3), and $\theta(x, y)$ is the q -distance between x, y (See Def. 2).

Proof. Using Sanov's theorem²⁸ on large deviations, we conclude that the probability of spontaneous jump from strain $x \in P$ to strain $y \in Q$, with the possibility $P \neq Q$, is given by:

$$Pr(x \rightarrow y) = \prod_{i=1}^N (\Phi_i^P(x_{-i})|y_i) \quad (20)$$

Writing the factors on the right hand side as:

$$\Phi_i^P(x_{-i})|y_i = \Phi_i^Q(y_{-i})|y_i \left(\frac{\Phi_i^P(x_{-i})|y_i}{\Phi_i^Q(y_{-i})|y_i} \right) \quad (21)$$

we note that $\Phi_i^P(x_{-i}), \Phi_i^Q(y_{-i})$ are distributions on the same index i , and hence:

$$|\Phi_i^P(x_{-i})|y_i - \Phi_i^Q(y_{-i})|y_i| \leq \sum_{y_i \in \Sigma_i} |\Phi_i^P(x_{-i})|y_i - \Phi_i^Q(y_{-i})|y_i| \quad (22)$$

Using a standard refinement of Pinsker's inequality⁵⁴, and the relationship of Jensen-Shannon divergence with total variation, we get:

$$\theta_i \geq \frac{1}{8} |\Phi_i^P(x_{-i})|y_i - \Phi_i^Q(y_{-i})|y_i|^2 \Rightarrow \left| 1 - \frac{\Phi_i^Q(y_{-i})|y_i}{\Phi_i^P(x_{-i})|y_i} \right| \leq \frac{1}{a_0} \sqrt{8\theta_i} \quad (23)$$

where a_0 is the smallest non-zero probability value of generating the entry at any index. We will see that this parameter is related to statistical significance of our bounds. First, we can formulate a lower bound as follows:

$$\log \left(\prod_{i=1}^N \frac{\Phi_i^P(x_{-i})|y_i}{\Phi_i^Q(y_{-i})|y_i} \right) = \sum_i \log \left(\frac{\Phi_i^P(x_{-i})|y_i}{\Phi_i^Q(y_{-i})|y_i} \right) \geq \sum_i \left(1 - \frac{\Phi_i^Q(y_{-i})|y_i}{\Phi_i^P(x_{-i})|y_i} \right) \geq \frac{\sqrt{8}}{a_0} \sum_i \theta_i^{1/2} = -\frac{\sqrt{8}N}{a_0} \theta \quad (24)$$

Similarly, the upper bound may be derived as:

$$\log \left(\prod_{i=1}^N \frac{\Phi_i^P(x_{-i})|y_i}{\Phi_i^Q(y_{-i})|y_i} \right) = \sum_i \log \left(\frac{\Phi_i^P(x_{-i})|y_i}{\Phi_i^Q(y_{-i})|y_i} \right) \leq \sum_i \left(\frac{\Phi_i^Q(y_{-i})|y_i}{\Phi_i^P(x_{-i})|y_i} - 1 \right) \leq \frac{\sqrt{8}N}{a_0} \theta \quad (25)$$

Combining Eqs. 24 and 25, we conclude:

$$\omega_y^Q e^{\frac{\sqrt{8}N}{a_0}\theta} \geq Pr(x \rightarrow y) \geq \omega_y^Q e^{-\frac{\sqrt{8}N}{a_0}\theta} \quad (26)$$

Now, interpreting a_0 as the probability of generating an unlikely event below our desired threshold (*i.e.* a "failure"), we note that the probability of generating at least one such event is given by $1 - (1 - a_0)^N$. Hence if α is the pre-specified significance level, we have for $N \gg 1$:

$$a_0 \approx (1 - \alpha)/N \quad (27)$$

Hence, we conclude, that at significance level $\geq \alpha$, we have the bounds:

$$\omega_y^Q e^{\frac{\sqrt{8}N^2}{1-\alpha}\theta} \geq Pr(x \rightarrow y) \geq \omega_y^Q e^{-\frac{\sqrt{8}N^2}{1-\alpha}\theta} \quad (28)$$

□

Remark 1. *This bound can be rewritten in terms of the log-likelihood of the spontaneous jump and constants independent of the initial sequence x as:*

$$|\log Pr(x \rightarrow y) - C_0| \leq C_1 \theta \quad (29)$$

where the constants are given by:

$$C_0 = \log \omega_y^Q \quad (30)$$

$$C_1 = \frac{\sqrt{8}N^2}{1-\alpha} \quad (31)$$

In-silico Corroboration of Emergenet's Capability To Capture Biologically Meaningful Structure

We compare the results of simulated mutational perturbations to sequences from our databases (for which we have already constructed Emergenets), and then use NCBI BLAST (<https://blast.ncbi.nlm.nih.gov/Blast.cgi>) to identify if our perturbed sequences match with existing sequences in the databases (Supplementary Fig. S-4). We find that in

contrast to random variations, which rapidly diverge the trajectories, the Emergenet constraints tend to produce smaller variance in the trajectories, maintain a high degree of match as we extend our trajectories, and produces matches closer in time to the collection time of the initial sequence, suggesting that the Emergenet does indeed capture realistic constraints.

Multivariate Regression to Understand Data Characteristics Necessary For Emergenet Modeling

We investigate the key factors that contribute to modeling a set of strains well within the Emergenet framework. We carry out a multivariate regression with data diversity, the complexity of inferred Emergenet and the edit distance of the WHO recommendation from a frequency-dominant strain as independent variables (See Supplementary Table S-7 for definitions). Here we define data diversity as the number of clusters we have in the input set of sequences, such that any two sequences five or less mutations apart are in the same cluster. Emergenet complexity is measured by the number of decision nodes in the component decision trees of the recursive forest.

We select several plausible structures of the regression equation, and in each case conclude that data diversity has the most important and statistically significant contribution (Supplementary Table S-7).

Extended Data Table 1
H1N1 northern hemisphere

Season	WHO Recommendation	Enet Recommendation, Cluster 1	Enet Recommendation, Cluster 2	Enet Recommendation, Single Cluster	WHO Error	Enet Error	Enet Error Single
2003-04	A/New Caledonia/20/99	A/Memphis/1/2001	A/HaNoi/2704/2002	A/Memphis/1/2001	8.3	5.3	11.3
2004-05	A/New Caledonia/20/99	A/Memphis/1/2001	A/Memphis/1/2001	A/Memphis/1/2001	7.4	9.7	9.7
2005-06	A/New Caledonia/20/99	A/Malaysia/25862/2003	A/Malaysia/25862/2003	A/Malaysia/25862/2003	10.6	6.4	6.4
2006-07	A/New Caledonia/20/99	A/Yazd/144/2006	A/Malaysia/30025/2004	A/New York/230/2003	10.4	5.7	6.4
2007-08	A/Solomon Islands/3/2006	A/New York/1050/2006	A/Incheon/2647/2007	A/New York/1050/2006	10.5	11.2	13.6
2008-09	A/Brisbane/59/2007	A/England/545/2007	A/Hong_Kong/2613/2007	A/England/545/2007	28.9	27.8	28.5
2009-10	A/Brisbane/59/2007	A/Hawaii/02/2008	A/Hong_Kong/H090-751-V3	A/Hawaii/02/2008	426.2	2.4*	426.2
2010-11	A/California/7/2009	A/OKINAWA/283/2009	A/Qingdao/FF86/2009	A/OKINAWA/283/2009	10.6	7.5	7.8
2011-12	A/California/7/2009	A/Florida/14/2010	A/Taiwan/66179/2010	A/Florida/14/2010	12.8	7.6	7.6
2012-13	A/California/7/2009	A/England/WTSI1769/2010	A/Mexico/3723/2011	A/Singapore/GP2892/2010	12.6	8.3	5.4
2013-14	A/California/7/2009	A/IIV-Vladimir/67/2011	A/Srinagar/827/2011	A/Helsinki/207/2013	14.5	5.8	7.7
2014-15	A/California/7/2009	A/Nicaragua/6184_13/2013	A/Nicaragua/6184_13/2013	A/Nicaragua/6184_13/2013	20.0	11.1	11.1
2015-16	A/California/7/2009	A/SENDAI/42/2014	A/USA/VFFSP_UNITHER_00011/2014	A/SENDAI/42/2014	16.8	6.9	6.9
2016-17	A/California/7/2009	A/Massachusetts/24/2015	A/India/1399/2015	A/Massachusetts/24/2015	17.9	3.7	3.7
2017-18	A/Michigan/45/2015	A/Bolzano/11/2016	A/Costa_Rica/4631/2016	A/Bolzano/11/2016	7.4	6.4	6.4
2018-19	A/Michigan/45/2015	A/Cambodia/B0629529/2017	A/Mississippi/26/2017	A/Qatar/16-VI-17-0046212/2017	10.3	6.2	5.3
2019-20	A/Brisbane/02/2018	A/Michigan/398/2018	A/Zambia/301/2017	A/Bhutan/15/2019	11.3	5.7	5.7
2020-21	A/Guangdong-Maonan/SWL1536/2019	A/Singapore/GP1719/2019	A/Baltimore/R0675/2019	A/Linkou/R0160/2018	17.1	10.7	11.5
2021-22	A/Victoria/2570/2019	A/Togo/64/2021	A/Tianjin/00030/2020	A/Togo/64/2021	10.8	8.4	8.4
2022-23	A/Victoria/2570/2019	A/Cameroon/7082/2021	A/England/221340346/2022	A/Lyon/CHU_0186413/2020	11.8	6.3	15.6
2023-24	A/Victoria/4897/2022	A/Bahrain/2446/2021	A/South_Africa/R05701/2022	A/South_Africa/14627/2021	-1	-1	-1

* A/Hong Kong/H090-751-V3, which is close to the 2009-10 H1N1 pandemic strain (5 edits), was collected on 2009-02-08, before the WHO recommendation was released, but submitted on 2011-07-08.

Extended Data Table 2
H1N1 southern hemisphere

Season	WHO Recommendation	Enet Recommendation, Cluster 1	Enet Recommendation, Cluster 2	Enet Recommendation, Single Cluster	WHO Error	Enet Error	Enet Error Single
2003	A/New Caledonia/20/99	A/HaNoi/2143/2001	A/HaNoi/2143/2001	A/HaNoi/2143/2001	7.3	3.0	3.0
2004	A/New Caledonia/20/99	A/HaNoi/2546/2002	A/HaNoi/2704/2002	A/HaNoi/2546/2002	11.2	8.8	10.8
2005	A/New Caledonia/20/99	A/Michigan/1/2003	A/Michigan/1/2003	A/Michigan/1/2003	8.7	5.8	5.8
2006	A/New Caledonia/20/99	A/Malaysia/25531/2003	A/Auckland/619/2005	A/Malaysia/25531/2003	12.9	9.7	10.6
2007	A/New Caledonia/20/99	A/Malaysia/1652509/2006	A/Malaysia/25531/2003	A/Malaysia/34291/2006	21.6	15.1	14.9
2008	A/Solomon Islands/3/2006	A/Malaysia/1715991/2007	A/Canada/0379/2007	A/New_York/08/2007	11.1	4.7	12.7
2009	A/Brisbane/59/2007	A/California/28/2007	A/Vietnam/100/2008	A/California/28/2007	402.0	401.2	402.1
2010	A/California/7/2009	A/Hong_Kong/H090-751-V3	A/Hawaii/02/2008	A/Hong_Kong/H090-751-V3	11.7	4.3	8.0
2011	A/California/7/2009	A/Guangdong/1250/2009	A/Kenya/1329/2010	A/Guangdong/1250/2009	10.5	6.7	6.7
2012	A/California/7/2009	A/Singapore/GP81/2011	A/Chongqing-Yuzhong/SWL11307/2009	A/Scotland/Inverness_10/2009	12.6	6.9	6.9
2013	A/California/7/2009	A/Virginia/07/2012	A/Kenya/CDC-KNH-028/2010	A/Singapore/GP4215/2010	13.3	6.5	9.2
2014	A/California/7/2009	A/England/358/2013	A/India/P1114854/2011	A/Cruz Alta/LACENRS-129/2012	13.8	4.3	2.5
2015	A/California/7/2009	A/North_Carolina/07/2013	A/shandong-zhifu/SWL1105/2014	A/North_Carolina/07/2013	14.9	4.1	4.1
2016	A/California/7/2009	A/Colombia/1457/2015	A/India/1399/2015	A/Cruz Alta/LACENRS-129/2012	16.8	4.2	5.0
2017	A/Michigan/45/2015	A/Ivanovo/CRIE-73/2016	A/Albania/6485/2016	A/Ivanovo/CRIE-73/2016	5.5	4.5	4.5
2018	A/Michigan/45/2015	A/Qatar/16-VI-17-0046212/2017	A/Chongqing-Yuzhong/SWL1453/2017	A/Texas/28/2016	8.8	3.9	5.9
2019	A/Michigan/45/2015	A/California/145/2017	A/California/145/2017	A/California/145/2017	11.2	6.3	6.3
2020	A/Brisbane/02/2018	A/Shanghai/192/2018	A/Germany/9054/2019	A/Nepal/19FL3860/2019	28.9	23.2	23.7
2021	A/Victoria/2570/2019	A/Yaroslavl/138/2020	A/Ontario/RV1058/2019	A/Qatar/16-VI-19-0068514/2019	11.6	12.0	11.1
2022	A/Victoria/2570/2019	A/Netherlands/10253/2020	A/India/PUN-NIV323483/2021	A/Mecklenburg-Vorpommern/2/2020	9.9	3.7	11.3
2023	A/Sydney/5/2021	A/Pakistan/GIHSN/ICT/826/2023	A/NIIGATA/922/2019	A/Pakistan/GIHSN/ICT/826/2023	-1	-1	-1

Extended Data Table 3
H3N2 northern hemisphere

Season	WHO Recommendation	Enet Recommendation, Cluster 1	Enet Recommendation, Cluster 2	Enet Recommendation, Single Cluster	WHO Error	Enet Error	Enet Error Single
2003-04	A/Moscow/10/99	A/Hong Kong/ CUHK53327/2002	A/Netherlands/88/2003	A/Hong Kong/ CUHK24044/2002	26.5	3.8	3.9
2004-05	A/Fujian/411/2002	A/Queensland/40/2003	A/Singapore/ NHRC0001/2003	A/New York/214/2003	10.4	5.7	7.5
2005-06	A/California/7/2004	A/Canterbury/18/2004	A/Tairawhiti/369/2004	A/Canterbury/18/2004	13.0	5.1	5.2
2006-07	A/Wisconsin/67/2005	A/Mexico/TLA2227/2005	A/New_York/1034/2006	A/Mexico/TLA2227/2005	10.9	5.7	8.5
2007-08	A/Wisconsin/67/2005	A/Mexico/MEX2640/2005	A/Madagascar/2694/2006	A/Kentucky/UR06-0044/2007	11.2	4.3	3.3
2008-09	A/Brisbane/10/2007	A/LangSon/LS218/2007	A/Malaysia/1767091/2007	A/LangSon/LS218/2007	5.0	2.3	2.4
2009-10	A/Brisbane/10/2007	A/Pennsylvania/PIT43/2008	A/Managua/5/2007	A/Pennsylvania/PIT43/2008	9.2	7.2	7.2
2010-11	A/Perth/16/2009	A/Stockholm/89/2009	A/Bordeaux/1942/2009	A/California/VRDL384/2009	10.4	8.0	6.9
2011-12	A/Perth/16/2009	A/Quebec/RV2804/2010	A/Mumbai/2516/2009	A/Singapore/N1604/2009	10.6	7.8	7.9
2012-13	A/Victoria/361/2011	A/Singapore/C2011.573/2011	A/Idaho/01/2010	A/Cote_d'Ivoire/ GR1596/2010	6.9	7.9	9.1
2013-14	A/Victoria/361/2011	A/Boston/DOA2-162/2012	A/Belem/119244/2012	A/Boston/DOA2-162/2012	8.8	4.0	4.0
2014-15	A/Texas/50/2012	A/Schleswig_Holstein/7/2012	A/Maryland/03/2014	A/Schleswig_Holstein/7/2012	10.7	2.9	9.8
2015-16	A/Switzerland/9715293/2013	A/New Hampshire/08/2014	A/Ireland/14M02879/2014	A/Thailand/CU-B11417/2014	10.6	5.7	5.5
2016-17	A/Hong Kong/4801/2014	A/Alaska/123/2015	A/Beijing-Xicheng/ 13100/2014	A/New_Hampshire/09/2014	6.2	6.9	7.1
2017-18	A/Hong Kong/4801/2014	A/South_Africa/R3703/2016	A/South_Africa/3731/2016	A/Tanzania/2220/2016	6.2	7.5	7.7
2018-19	A/Singapore/INFIMH-16-0019/2016	A/Hong_Kong/3554/2017	A/Taiwan/473/2017	A/Connecticut/21/2014	12.7	10.5	12.7
2019-20	A/Kansas/14/2017	A/Maldives/338/2018	A/Tennessee/64/2018	A/Arkansas/15/2016	13.7	5.2	12.5
2020-21	A/Hong Kong/2671/2019	A/Alaska/04/2019	A/Guangxi-Mashan/32/2019	A/Colombia/5215/2015	15.9	15.7	21.9
2021-22	A/Cambodia/e0826360/2020	A/Bangladesh/1003/2020	A/Nigeria/4976/2020	A/Nepal/21FL0201/2021	16.3	7.4	7.5
2022-23	A/Darwin/9/2021	A/Saarland/1/2022	A/Nepal/21FL2439/2021	A/Darwin/7/2021	8.2	7.1	6.5
2023-24	A/Darwin/9/2021	A/Michigan/ UOM10045676784/2022	A/Norway/34811/2022	A/Texas/78/2022	-1	-1	-1

Extended Data Table 4
H3N2 southern hemisphere

Season	WHO Recommendation	Enet Recommendation, Cluster 1	Enet Recommendation, Cluster 2	Enet Recommendation, Single Cluster	WHO Error	Enet Error	Enet Error Single
2003	A/Moscow/10/99	A/Canterbury/09/2002	A/Hong_Kong/ CUHK24167/2002	A/Canterbury/57/2002	26.0	6.6	17.9
2004	A/Fujian/411/2002	A/Wellington/3/2003	A/Hong_Kong/ CUHK6377/2003	A/Queensland/40/2003	9.3	7.3	7.3
2005	A/Wellington/1/2004	A/Canterbury/11/2004	A/TayNguyen/TN905/2003	A/Canterbury/11/2004	6.7	4.0	4.1
2006	A/California/7/2004	A/Hong Kong/ CUHK7711/2005	A/New Jersey/ NHRC0001/2005	A/Canterbury/11/2004	13.6	2.9	4.6
2007	A/Wisconsin/67/2005	A/Mexico/DIF2601/2005	A/Illinois/NHRC0002/2006	A/Mexico/DIF2601/2005	12.0	8.2	8.3
2008	A/Brisbane/10/2007	A/Washington/UR06-0225/2007	A/Australia/NHRC0013/2005	A/Washington/UR06-0225/2007	4.9	5.8	5.8
2009	A/Brisbane/10/2007	A/Kentucky/UR07-0124/2008	A/Argentina/405/2007	A/Vietnam/214/2008	7.9	5.9	5.9
2010	A/Perth/16/2009	A/Hong_Kong/H090-755-V2	A/Sydney/3/2009	A/California/VRDL255/2009	8.9	8.8	8.0
2011	A/Perth/16/2009	A/Bangladesh/483/2009	A/Singapore/C2010.310/2010	A/Singapore/C2009.784/2009	10.0	5.5	6.6
2012	A/Perth/16/2009	A/Uganda/UVRI/Kisenyi/ 005/2010-09-28	A/Romania/55656/2011	A/California/VRDL384/2009	17.5	12.4	14.3
2013	A/Victoria/361/2011	A/Alborz/1095/2012	A/West Virginia/06/2011	A/Kentucky/21/2009	8.1	8.9	12.8
2014	A/Texas/50/2012	A/Niakhar/7504/2012	A/Houston/JMM_77/2012	A/New_York/05/2013	8.8	6.4	6.7
2015	A/Switzerland/9715293/2013	A/Trinidad/3558/2013	A/Singapore/G2-6.1/2013	A/Boston/DOA2-162/2012	10.7	11.4	9.9
2016	A/Hong Kong/4801/2014	A/Scotland/146/2015_(H3N2)	A/Barbados/2879/2015	A/Scotland/146/2015_(H3N2)	6.9	5.3	7.6
2017	A/Hong Kong/4801/2014	A/Taiwan/1098/2015	A/Mexico/2117/2015	A/VICTORIA/5070/2014	7.6	8.2	8.5
2018	A/Singapore/INFIMH-16-0019/2016	A/FUKUSHIMA/122/2016	A/Alberta/RV0043/2016	A/Tanzania/2220/2016	9.6	6.4	8.8
2019	A/Switzerland/8060/2017	A/England/7400/2018	A/Singapore/SGH0650/2017	A/Heilongjiang-Xiangyang/11347/2015	15.9	10.2	14.0
2020	A/South Australia/34/2019	A/Alicante/ 19_2105_20190326	A/Jiangsu-Rugao/326/2018	A/Singapore/KK1149/2017	12.0	14.2	10.9
2021	A/Hong Kong/2671/2019	A/Cambodia/e0826360/2020	A/Bangladesh/8001/2020	A/Indonesia/ NIHRDLP854/2020	18.3	9.1	12.9
2022	A/Darwin/9/2021	A/India/PUN-NIV301718/2021	A/Marseille/0486/2021_aug	A/Bangladesh/0002/2020	7.1	5.3	6.7
2023	A/Darwin/9/2021	A/Bulgaria/1666/2022	A/Michigan/ UOM10045976087/2022	A/Bulgaria/1666/2022	-1	-1	-1

Extended Data Table 5
Out-performance of Emergenet recommendations over WHO for Influenza A vaccine composition

Subtype	Hemisphere	Cluster	Two decades			One decade		
			WHO Error	Enet Error	Improvement %	WHO Error	Enet Error	Improvement %
H1N1	North	1	13.15* (33.80)	9.42* (30.26)	28.40* (11.73)	13.78	8.24	67.27
H1N1	North	2	13.15* (33.80)	8.46* (8.15)	35.71* (314.64)	13.78	7.13	93.29
H1N1	South	1	12.76* (32.22)	8.57* (28.25)	32.81* (14.07)	13.47	8.35	61.31
H1N1	South	2	12.76* (32.22)	7.24* (26.93)	43.29* (19.64)	13.47	7.26	85.59
H3N2	North	1	11.18	7.86	42.13	10.94	9.53	14.72
H3N2	North	2	11.18	6.54	70.86	10.94	7.29	49.93
H3N2	South	1	11.08	9.07	22.11	10.49	9.88	6.22
H3N2	South	2	11.08	7.65	44.94	10.49	8.55	22.73

* Average omits the 2009-10 H1N1 pandemic season. Complete average in parentheses.

Extended Data Table 6
Emergenet against Huddleston et al.⁶ predictions; reported improvement over WHO distance to future

Timepoint	WHO Recommendation	Emergenet Distance to Future	Emergenet Improvement	LBI + Mutational Load Distance to Future	LBI + Mutational Load Improvement	HI + Mutational Load Distance to Future	HI + Mutational Load Improvement
2003-10-01	A/Fujian/411/2002	7.28	2.05	8.44	1.01	6.50	2.95
2004-10-01	A/Wellington/1/2004	4.06	2.63	4.38	1.70	4.38	1.70
2005-04-01	A/California/7/2004	5.18	7.82	4.60	2.89	4.60	2.89
2006-04-01	A/Wisconsin/67/2005	8.54	2.36	5.36	4.94	5.37	4.94
2007-10-01	A/Brisbane/10/2007	5.78	-0.88	3.78	2.00	3.78	2.00
2009-10-01	A/Perth/16/2009	8.03	0.83	6.95	1.00	7.93	0.02
2012-04-01	A/Victoria/361/2011	4.00	4.79	3.72	2.54	7.02	-0.75
2013-10-01	A/Texas/50/2012	6.66	2.10	6.54	2.11	6.89	1.76
2014-10-01	A/Switzerland/9715293/2013	9.85	0.87	3.88	6.94	3.88	6.94
2015-10-01	A/Hong Kong/4801/2014	7.64	-0.74	7.33	-1.24	6.09	0.00
2017-10-01	A/Singapore/INFIMH-16-0019/2016	8.79	0.78	7.47	1.15	7.81	0.80
2018-10-01	A/Switzerland/8060/2017	13.97	1.94	17.08	-1.91	10.42	4.75
	Average	7.48	2.05	6.63	1.93	6.22	2.33

* Our strain population is slightly different, so our WHO distance to the future is also slightly different. You can retrieve our WHO distance to the future by adding the columns "Emergenet Distance to Future" and "Emergenet Improvement". Likewise, you can retrieve their distance to the future in a similar way.

Extended Data Table 7
Out-performance of Emergenet single-cluster recommendations over randomly selected strains

Subtype	Hemisphere	Two decades			One decade		
		Random Error	Enet Error	Improvement %	Random Error	Enet Error	Improvement %
H1N1	North	13.40* (34.03)	9.42* (30.26)	29.69* (12.49)	14.77	8.24	79.36
H1N1	South	15.88* (35.20)	8.57* (28.25)	46.03* (24.61)	14.50	8.35	73.54
H3N2	North	10.80	7.86	37.37	12.45	9.53	30.61
H3N2	South	12.30	9.07	35.54	12.87	9.88	30.26

* Average omits the 2009-10 H1N1 pandemic season. Complete average in parentheses.

Extended Data Table 8
Influenza A strains evaluated by IRAT and corresponding Emergenet predicted risk scores

Influenza Virus	Virus Type	Date of Risk Assessment	Risk Score Category	Emergence Score	Mean Low Acceptable Emergence	Mean High Acceptable Emergence	Geom Mean Risk	Predicted Emergence	Predicted Emergence Low	Predicted Emergence High
A/Hong Kong/125/2017	H7N9	2017-05-01	Moderate-High	6.5	5.65	7.51	0.00001	7.73	6.19	9.18
A/Shanghai/02/2013	H7N9	2016-04-01	Moderate-High	6.4	5.52	7.43	0.00001	7.73	6.19	9.18
A/California/62/2018	H1N2	2019-07-01	Moderate	5.8	4.22	7.16	0.00001	7.73	6.19	9.18
A/Indiana/08/2011	H3N2	2012-12-01	Moderate	6.0	-1	-1	0.00005	7.66	6.13	9.1
A/Sichuan/06681/2021	H5N6	2021-10-01	Moderate	5.3	3.88	6.45	0.00128	6.58	5.2	7.92
A/Anhui-Luijiang/39/2018	H9N2	2019-07-01	Moderate	6.2	4.76	7.57	0.00163	6.42	5.06	7.74
A/Ohio/13/2017	H3N2	2019-07-01	Moderate	6.6	5.01	7.59	0.00200	6.27	4.93	7.58
A/mink/Spain/3691-8_22VIR10586-10/2022	H5N1	2023-04-01	Moderate	5.1	3.96	6.27	0.00264	6.07	4.75	7.35
A/swine/Shandong/1207/2016	H1N1	2020-07-01	Moderate	7.5	6.33	8.65	0.00315	5.93	4.64	7.2
A/Vietnam/1203/2004	H5N1	2011-11-01	Moderate	5.2	-1	-1	0.00505	5.54	4.31	6.78
A/American wigeon/South Carolina/AH0195145/2021	H5N1	2022-03-01	Moderate	4.4	3.28	5.51	0.00692	5.28	4.08	6.49
A/Northern pintail/Washington/40964/2014	H5N2	2015-03-01	Low-Moderate	3.8	2.6	5.0	0.01381	4.68	3.56	5.83
A/American green-winged teal/Washington/1957050/2014	H5N1	2015-03-01	Low-Moderate	3.6	2.4	4.6	0.01484	4.61	3.5	5.76
A/canine/Illinois/12191/2015	H3N2	2016-06-01	Low	3.7	2.81	4.9	0.01750	4.46	3.38	5.6
A/Bangladesh/0994/2011	H9N2	2014-02-01	Moderate	5.6	4.49	6.74	0.03224	3.92	2.91	4.99
A/Yunnan/14564/2015	H5N6	2016-04-01	Moderate	5.0	4.07	6.18	0.04202	3.68	2.7	4.73
A/gyrfalcon/Washington/41088/2014	H5N8	2015-03-01	Low-Moderate	4.2	2.9	5.3	0.05259	3.47	2.53	4.51
A/chicken/Tennessee/17-007431-3/2017	H7N9	2017-10-01	Low	3.1	2.2	3.94	0.05422	3.45	2.5	4.48
A/Jiangxi-Donghu/346/2013	H10N8	2014-02-01	Moderate	4.3	3.37	5.96	0.06794	3.24	2.32	4.25
A/turkey/Indiana/1573-2/2016	H7N8	2017-07-01	Low	3.4	2.4	4.26	0.07830	3.11	2.21	4.11
A/chicken/Tennessee/17-007147-2/2017	H7N9	2017-10-01	Low	2.8	2.01	3.71	0.07995	3.09	2.2	4.09
A/Astrakhan/3212/2020	H5N8	2021-03-01	Moderate	4.6	3.64	5.82	0.13983	2.58	1.76	3.53
A/Netherlands/219/2003	H7N7	2012-06-01	Moderate	4.6	3.22	4.39	0.14384	2.56	1.74	3.50

* First seven columns available from IRAT¹⁶. Last four columns predicted by Emergenet.

** The strain A/duck/New York/1996, analyzed by IRAT to have emergence score 2.3 on 2011-11-01, is omitted because its HA segment is unavailable.

Extended Data Table 9
Count of identified animal strains above estimated emergence risk threshold

Subtype	Score > 6.5	Score > 7.0	Score > 7.5	Score > 7.7
H1N1	7 (8.75%)	3 (25.0%)	2 (33.33%)	1 (25.0%)
H3N2	14 (17.5%)	3 (25.0%)	2 (33.33%)	1 (25.0%)
H7N9	1 (1.25%)	1 (8.33%)	1 (16.67%)	1 (25.0%)
H9N2	0 (0.0%)	0 (0.0%)	0 (0.0%)	0 (0.0%)
H5N1	49 (61.25%)	3 (25.0%)	0 (0.0%)	0 (0.0%)
H1N2	8 (10.0%)	2 (16.67%)	1 (16.67%)	1 (25.0%)
H3N3	1 (1.25%)	0 (0.0%)	0 (0.0%)	0 (0.0%)

Extended Data Table 10

Influenza A strains evaluated by IRAT and corresponding Emergenet predicted risk scores, sampling 75% of strains from each subtype in the current human population (averaged over 20 random seeds)

Influenza Virus	Virus Type	Date of Risk Assessment	Risk Score Category	Emergence Score	Geom Mean Risk	Geom Mean Risk SEM	Predicted Emergence	Predicted Emergence SEM	Predicted Emergence W/O Sampling
A/Hong Kong/125/2017	H7N9	2017-05-01	Moderate-High	6.5	0.00001	0.00000	7.73	0.00000	7.73
A/California/62/2018	H1N2	2019-07-01	Moderate	5.8	0.00001	0.00000	7.73	0.00000	7.73
A/Shanghai/02/2013	H7N9	2016-04-01	Moderate-High	6.4	0.00002	0.00001	7.72	0.01700	7.73
A/Indiana/08/2011	H3N2	2012-12-01	Moderate	6.0	0.00028	0.00007	7.4	0.06600	7.67
A/Ohio/13/2017	H3N2	2019-07-01	Moderate	6.6	0.00227	0.00010	6.19	0.02900	6.27
A/Anhui-Luijiang/39/2018	H9N2	2019-07-01	Moderate	6.2	0.00327	0.00029	5.95	0.06900	6.42
A/swine/Shandong/1207/2016	H1N1	2020-07-01	Moderate	7.5	0.00366	0.00047	5.9	0.09000	5.93
A/mink/Spain/3691-8_22VIR10586-10/2022	H5N1	2023-04-01	Moderate	5.1	0.00371	0.00059	5.99	0.14100	6.06
A/canine/Illinois/12191/2015	H3N2	2016-06-01	Low	3.7	0.00854	0.00101	5.18	0.08200	4.46
A/Northern pintail/Washington/40964/2014	H5N2	2015-03-01	Low-Moderate	3.8	0.00920	0.00103	5.11	0.08500	4.67
A/Sichuan/06681/2021	H5N6	2021-10-01	Moderate	5.3	0.01089	0.00640	5.9	0.25200	6.58
A/American green-winged teal/Washington/1957050/2014	H5N1	2015-03-01	Low-Moderate	3.6	0.02009	0.00108	4.36	0.04400	4.61
A/Bangladesh/0994/2011	H9N2	2014-02-01	Moderate	5.6	0.02494	0.00260	4.21	0.06900	3.92
A/Vietnam/1203/2004	H5N1	2011-11-01	Moderate	5.2	0.03444	0.00184	3.88	0.04600	5.54
A/Yunnan/14564/2015	H5N6	2016-04-01	Moderate	5.0	0.03817	0.00250	3.8	0.05900	3.68
A/gyrfalcon/Washington/41088/2014	H5N8	2015-03-01	Low-Moderate	4.2	0.03849	0.00224	3.79	0.06200	3.47
A/Jiangxi-Donghu/346/2013	H10N8	2014-02-01	Moderate	4.3	0.05588	0.00553	3.5	0.08700	3.24
A/turkey/Indiana/1573-2/2016	H7N8	2017-07-01	Low	3.4	0.05800	0.00512	3.45	0.08500	3.11
A/chicken/Tennessee/17-007431-3/2017	H7N9	2017-10-01	Low	3.1	0.05819	0.00524	3.47	0.10400	3.45
A/American wigeon/South Carolina/AH0195145/2021	H5N1	2022-03-01	Moderate	4.4	0.06305	0.00707	3.46	0.13100	5.28
A/chicken/Tennessee/17-007147-2/2017	H7N9	2017-10-01	Low	2.8	0.07537	0.00629	3.24	0.10900	3.09
A/Netherlands/219/2003	H7N7	2012-06-01	Moderate	4.6	0.09285	0.00821	3.03	0.08700	2.56
A/Astrakhan/3212/2020	H5N8	2021-03-01	Moderate	4.6	0.15732	0.00509	2.48	0.02800	2.58

* First five columns available from IRAT¹⁶. Last five columns predicted by Emergenet.

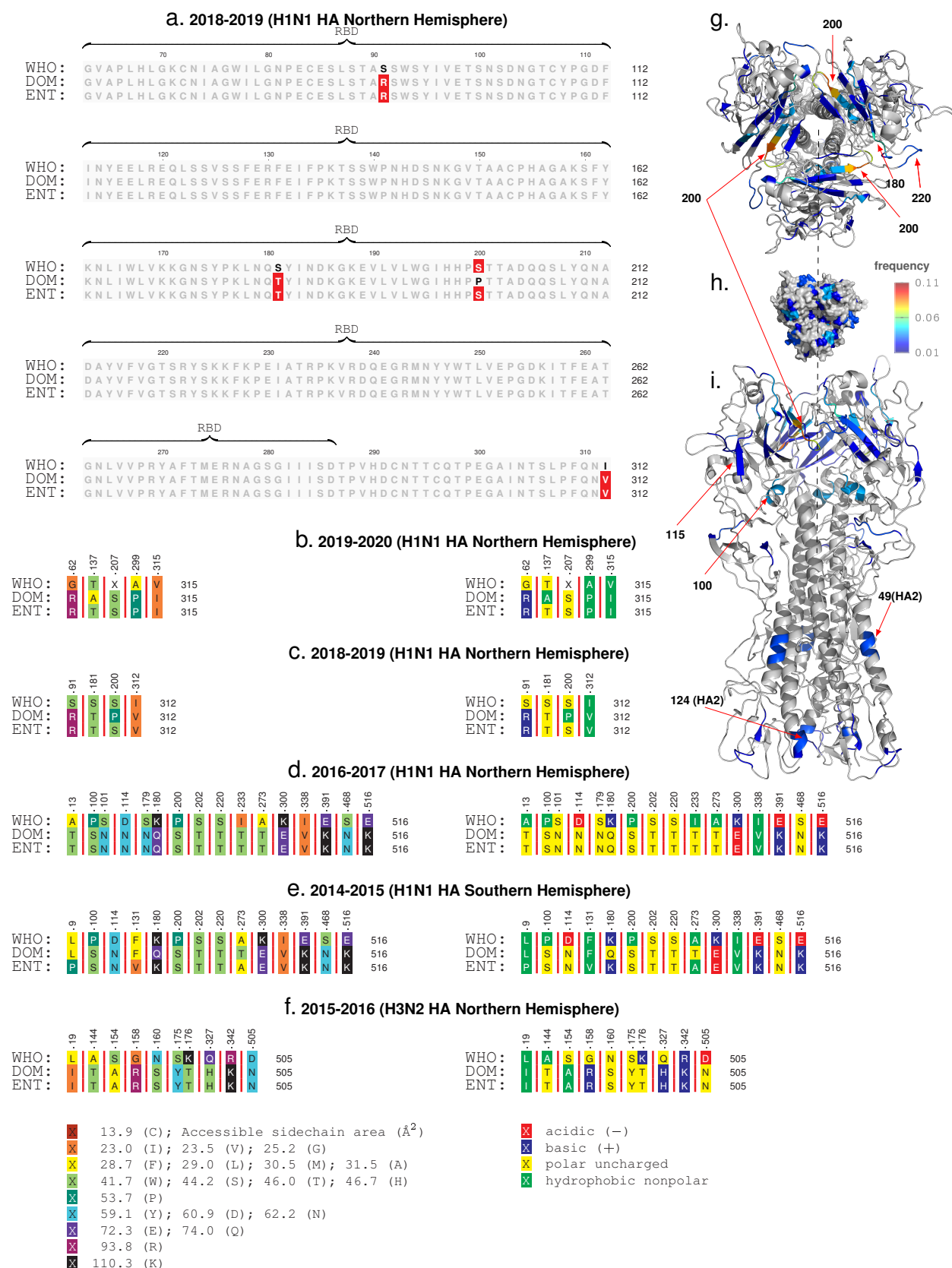
** The strain A/duck/New York/1996, analyzed by IRAT to have emergence score 2.3 on 2011-11-01, is omitted because its HA segment is unavailable.

Extended Data Table 11

Baseline performance with naive sequence match: correlation with 95% confidence bounds of edit distance between animal strains and high fitness human strains (H1N1). Sequence match with edit distance metric was limited to the RBD, and specific biologically important residue locations within the RBD

	HA E-distance (2020-2022 sequences)	Geometric mean of HA and NA E-distance (2020-2022 sequences)	HA E-distance (IRAT sequences)	Geometric mean of HA and NA E-distance (IRAT sequences)	CDC computed IRAT emergence score
On RBD (63-286)	0.671 ± 0.005	0.773 ± 0.007	0.214 ± 0.061	0.376 ± 0.071	-0.43
On selected residues on RBD*	-0.21 ± 0.007	-0.203 ± 0.01	-0.545 ± 0.02	-0.234 ± 0.03	-0.16
On 220 loop (210-240)	-0.052 ± 0.00	-0.131 ± 0.00	-0.523 ± 0.09	-0.172 ± 0.07	-0.15

* Residue positions 130,131,132,133,134,135,150,151,152,153,154,155,156,157,158,159,160,190,191,192,193,194,195,220,221,222,223,224,225,226, comprising the 190-helix, the 150-loop, the 220-loop and the 130-loop, which are known to play key role in HA function⁵⁷



Extended Data Figure 1. **Sequence comparisons.** Panel a Comparing the Emergenet (ENT) and the WHO recommendation (WHO), and the observed dominant strain (DOM), we note that the correct Emergenet predictions tend to be within the RBD, both for H1N1 and H3N2 for HA. Panels b-f Additionally, by comparing the type, side chain area, and the accessible side chain area, we note that DOM and ENT are often close in important chemical properties, while WHO deviations are not. Panels g-i show the localization of the deviations in the molecular structure of HA, where we note that the changes are most frequent in the HA1 sub-unit (the globular head), and around residues and structures that have been commonly implicated in receptor binding interactions *e.g* the \approx 200 loop, the \approx 220 loop and the \approx 180-helix⁵⁸⁻⁶⁰.

Extended Data Table 12
 Top ranked risky strains amongst 6, 354 animal strains collected post-2020 unique upto 15 edits in HA sequence

Strain	Subtype	HA accession	NA accession	Predicted IRAT emergence
A/Shanghai/02/2013	H7N9	EPI448936	EPI448938	7.7327
A/swine/North_Carolina/A02751333/2022	H3N2	EPI2396893	EPI2396894	7.7327
A/swine/Iowa/CEIRS-1495/2023	H1N2	EPI2908633	EPI2908631	7.7327
A/swine/Tver_region/RII-81-1S/2023	H1N1	EPI2965146	EPI2965145	7.7327
A/Indiana/08/2011	H3N2	EPI344405	EPI344404	7.6364
A/swine/North_Carolina/A02479173/2020	H1N1	EPI1780425	EPI1780426	7.5991
A/Common_Buzzard/England/125155/2023	H5N1	EPI2574053	EPI2574052	7.4234
A/backyard_chicken/Uruguay/UDELAR-144-M3/2023	H5N1	EPI2758928	EPI2758926	7.4152
A/Tufted_duck/Netherlands/1/2023	H5N1	EPI2904803	EPI2904802	7.4125
A/swine/Iowa/A02479084/2020	H1N2	EPI1779472	EPI1779473	7.3386
A/swine/Minnesota/A02245579/2020	H3N2	EPI1775813	EPI1775814	7.2054
A/swine/ISU-Illinois/A02861867/2023	H1N1	EPI2908017	EPI2908016	7.1952
A/swine/Iowa/A02751092/2022	H1N1	EPI2381136	EPI2381137	6.9698
A/peregrine_falcon/Netherlands/22000191-001/2022	H5N1	EPI1980868	EPI1980867	6.9508
A/otter/Finland/2860_21VIR9619-5/2021	H5N1	EPI2197232	EPI2197231	6.9362
A/swine/North_Carolina/A02751482/2023	H1N2	EPI2456343	EPI2456344	6.9019
A/gull/Estonia/TA2113284-4_21VIR7512-8/2021	H5N1	EPI1945389	EPI1945388	6.8990
A/lynx/Finland/Vi209-22_22VIR3127-2/2022	H5N1	EPI2197224	EPI2197223	6.8905
A/domestic_duck/England/076401/2021	H5N1	EPI2071928	EPI2071927	6.8736
A/swine/Illinois/A02525253/2021	H3N2	EPI1910375	EPI1910376	6.8375
A/swine/South_Korea/GNJJ/2020	H1N2	EPI2258341	EPI2258343	6.8270
A/Great_skua/Iceland/2023A104253/2022	H5N1	EPI2635214	EPI2635213	6.8097
A/Gyrfalcon/Iceland/2023A104255/2022	H5N1	EPI2635279	EPI2635277	6.8093
A/herring_gull/England/248639/2022	H5N1	EPI2158600	EPI2158599	6.8089
A/chicken/England/085598/2022	H5N1	EPI2089022	EPI2089021	6.8089
A/lesser_black-backed_gull/Netherlands/22012469-002/2022	H5N1	EPI2137792	EPI2137790	6.8089
A/Anser_anser/Spain/1035-5_22VIR6312-8/2022	H5N1	EPI2102649	EPI2102648	6.8089
A/Mallard/Netherlands/18/2022	H5N1	EPI2197857	EPI2197856	6.8089
A/turkey/Italy/21VIR10251/2021	H5N1	EPI1944389	EPI1944388	6.8089
A/grey_heron/Netherlands/21038941-001/2021	H5N1	EPI1941418	EPI1941417	6.8089
A/duck/France/21343/2021	H5N1	EPI2536840	EPI2536875	6.8089
A/duck/Spain/2095-2_22VIR8632-5/2022	H5N1	EPI2191149	EPI2191148	6.8085
A/goose/France/22P004055/2022	H5N1	EPI2780410	EPI2780409	6.8072
A/turkey/Poland/H1923_21RS3290-1/2021	H5N1	EPI2782408	EPI2782407	6.8070
A/laying_hen/Italy/21VIR11168/2021	H5N1	EPI2140973	EPI2140972	6.8066
A/turkey/Italy/21VIR8585-1/2021	H5N1	EPI1923192	EPI1923194	6.8066
A/chicken/Czech_Republic/61-1/2022	H5N1	EPI1999361	EPI1999360	6.8066
A/turkey/Italy/21VIR10001/2021	H5N1	EPI2139999	EPI2139998	6.8066
A/chicken/Italy/21VIR9940-5/2021	H5N1	EPI2140039	EPI2140038	6.8066
A/chicken/Italy/21VIR10094/2021	H5N1	EPI2140083	EPI2140082	6.8053
A/chicken/Italy/21VIR10263/2021	H5N1	EPI2140199	EPI2140198	6.8043
A/goose/Czech_Republic/25322-179/2021	H5N1	EPI2021894	EPI2021896	6.8035
A/broiler/Italy/21VIR11886-1/2021	H5N1	EPI2141602	EPI2141601	6.8025
A/swine/France/59-200284/2020	H1N2	EPI1976498	EPI1976500	6.8016
A/swan/Slovenia/2049_22VIR777-3/2021	H5N1	EPI1995084	EPI1995083	6.8003
A/turkey/Italy/21VIR10852/2021	H5N1	EPI2140553	EPI2140552	6.7956
A/turkey/Wales/065047/2021	H5N1	EPI2071520	EPI2071519	6.7830
A/chicken/Luxembourg/23023602/2023	H5N1	EPI2364554	EPI2364572	6.7826
A/Common_Teal/Netherlands/1/2022	H5N1	EPI2185431	EPI2185430	6.7823
A/Common_Tern/Netherlands/12/2022	H5N1	EPI2119243	EPI2119242	6.7804
A/turkey/Spain/140-38_22VIR2142-19/2022	H5N1	EPI1998202	EPI1998201	6.7697
A/swine/Minnesota/A02524797/2020	H3N2	EPI1907265	EPI1907266	6.7679
A/canine/Pennsylvania/CVM-985419/2023	H3N2	EPI2906952	EPI2906950	6.7569
A/Herring_gull/France/22P019328/2022	H5N1	EPI2780738	EPI2780737	6.7308
A/otter/Netherlands/22001014-005/2022	H5N1	EPI1965229	EPI1965228	6.7203
A/Harbour_Seal/Scotland/162919/2022	H5N1	EPI2398403	EPI2398402	6.7092
A/swine/Denmark/S20996-3/2021	H1N2	EPI1980810	EPI1980812	6.7069
A/swine/Germany/2021A104886/2021_(H1pdmN2	H1N2	EPI2551752	EPI2551751	6.6937
A/American_Crow/BC/AIVPHL-1468/2023	H5N1	EPI2856554	EPI2856544	6.6846
A/chicken/Italy/21VIR10812-11/2021	H5N1	EPI2140660	EPI2140658	6.6807
A/great_crested_grebe/Netherlands/22001219-002/2022	H5N1	EPI1990440	EPI1990439	6.6777
A/fox/England/015850/2022	H5N1	EPI2437468	EPI2437467	6.6711
A/swine/Germany/2022A100363/2022_(H1avN1)	H1N1	EPI2551584	EPI2551583	6.6577
A/barnacle_goose/Netherlands/22007405-004/2022	H5N1	EPI2028769	EPI2028768	6.6518
A/swine/England/129502/2023	H1N2	EPI2818798	EPI2818800	6.6469
A/swine/Iowa/ISU-A02862194/2023	H3N2	EPI2971632	EPI2971631	6.6454
A/swine/Iowa/A02636162/2021	H1N1	EPI1932974	EPI1932975	6.6453
A/swine/Iowa/ISU-A02861853/2023	H3N2	EPI2874299	EPI2874298	6.6389



Extended Data Figure 2. **High-risk animal strain comparison.** HA sequence comparison with 2020-2021 dominant frequency human strains (A/Baltimore/JH/001/2021, A/Myanmar/I026/2021, A/Darwin/12/2021) with Emergenet estimated top H3N2 risky strain EPI1818137 (emergence score > 7.26, 2020-2022 April) showing differences in and out of the RBD.

SUPPLEMENTARY FIGURES & TABLES

S-Tab. 1
Number of Influenza sequences collected from public databases

Database	Influenza Subtype	No. HA Sequences	No. NA Sequences	Total
GISAID	H1N1	73,905	73,920	147,825
NCBI	H1N1	18,577	16,913	35,490
GISAID	H3N2	108,829	108,860	217,689
NCBI	H3N2	18,840	15,249	34,089
GISAID	H1N2	1,340	1,340	2,680
GISAID	H1N7	18	18	36
GISAID	H3N8	406	405	811
GISAID	H4N6	68	68	136
GISAID	H5N1	8,245	8,145	16,390
GISAID	H5N2	35	35	70
GISAID	H5N3	44	43	87
GISAID	H5N5	74	74	148
GISAID	H5N6	282	282	564
GISAID	H5N8	1,561	1,513	3,074
GISAID	H6N1	31	31	62
GISAID	H6N2	47	41	88
GISAID	H6N6	62	62	124
GISAID	H7N3	122	120	242
GISAID	H7N9	1,274	1,273	2,547
GISAID	H9N2	451	451	902
GISAID	H10N3	43	43	86
GISAID	H10N7	15	15	30
GISAID	H11N9	33	33	66
GISAID	H13N6	15	15	30
Both	Total	234,317	228,949	463,266

S-Tab. 2
Examples: Emergenet induced distance varying for fixed sequence pair when background population changes (rows 1-5), sequences with small edit distance and large E-distance, and the converse (rows 6-9)

Hamming Distance	Sequence A	Sequence B	Emergenet E-Distance	Year A*	Year B*
18	A/Singapore/23J/2007	A/Tennessee/UR06-0294/2007	0.0111	2007	2007
18	A/Singapore/23J/2007	A/Tennessee/UR06-0294/2007	0.0094	2008	2008
18	A/Singapore/23J/2007	A/Tennessee/UR06-0294/2007	0.0027	2009	2009
18	A/Singapore/23J/2007	A/Tennessee/UR06-0294/2007	0.0025	2010	2010
18	A/Singapore/23J/2007	A/Tennessee/UR06-0294/2007	0.6163	2007	2010
11	A/Naypyitaw/M783/2008	A/Singapore/201/2008	0.8852	2008	2008
15	A/Cambodia/W0908339/2012	A/Singapore/DMS1233/2012	0.2737	2012	2012
126	A/South Dakota/03/2008	A/Singapore/10/2008	0.3034	2008	2008
141	A/Jodhpur/3248/2012	A/Cambodia/W0908339/2012	0.2405	2012	2012

* Year A and year B correspond to the assumed collection years for sequences A and B respectively for the purpose of this example. Sequence A in row 1 is collected in 2007, but is assumed to be from different years in rows 2-4 to demonstrate the change in E-distance from sequence B, arising only from a change in the background population.

S-Tab. 3
Correlation between E-distance and edit distance between sequence pairs

Phenotypes	Correlation
Influenza H1N1 HA	0.76
Influenza H1N1 NA	0.74
Influenza H3N2 HA	0.85
Influenza H3N2 NA	0.79



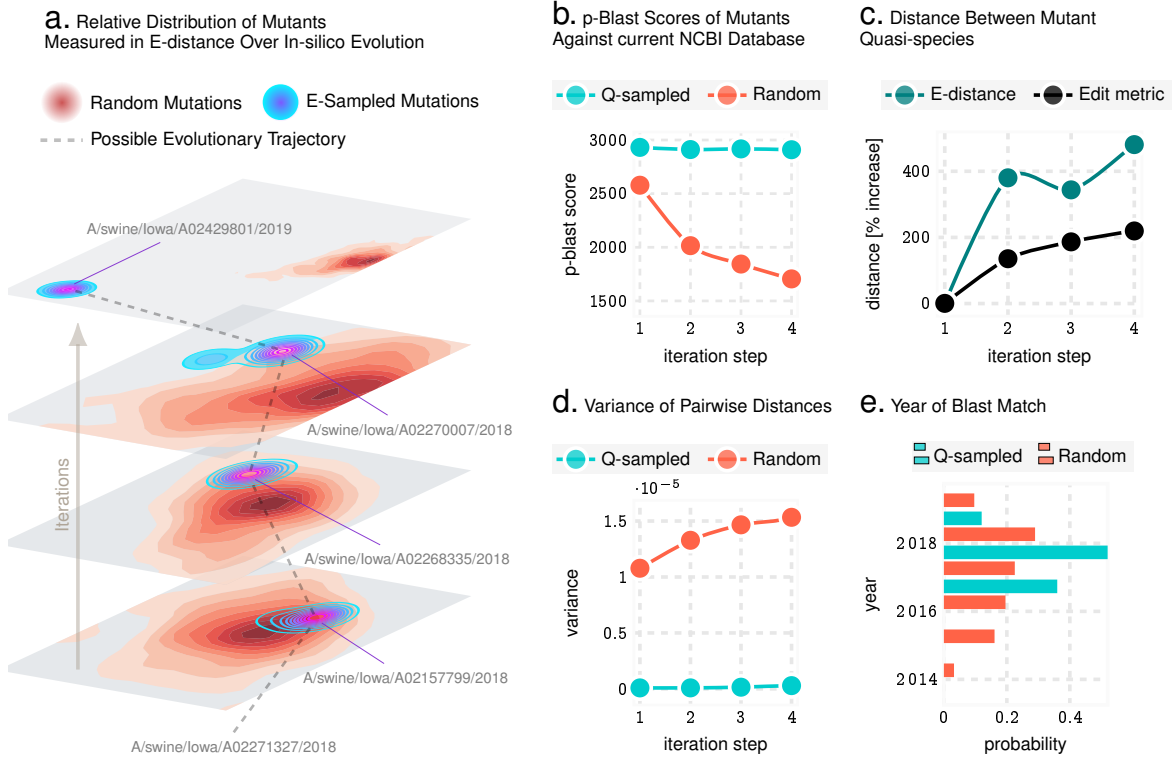
S-Fig. 1. **Low-risk animal strain comparison.** HA sequence comparison with 2020-2021 dominant frequency human strains (A/Baltimore/JH/001/2021, A/Myanmar/1026/2021, A/Darwin/12/2021) with Emergenet estimated relatively medium-risk H3N2 EPI2146849 (emergence risk score 6.5) showing substantially more differences compared to high-risk strain comparison shown in Extended Data Fig. 1.



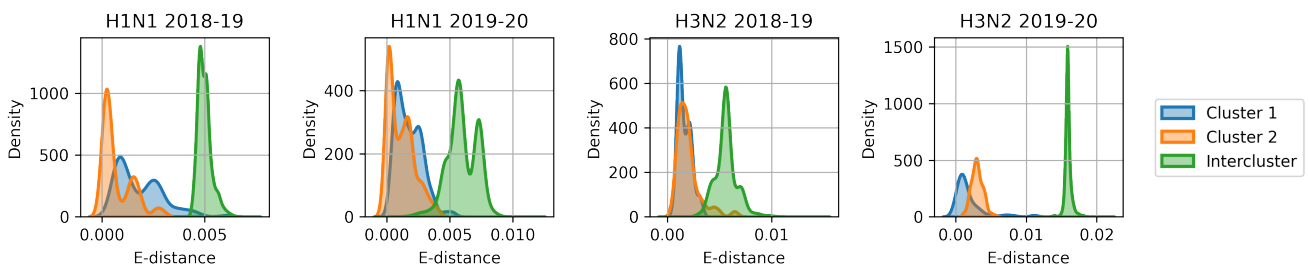
S-Fig. 2. **High-risk comparison.** HA sequence comparison with dominant frequency human strains (A/Togo/0172/2021, A/Bangladesh/9004/2021, A/Wisconsin/04/2021) with Emergenet estimated top H1N1 risky strain EPI1818121 (2020-2022 April, emergence score 7.69) showing differences both in and out of the RBD.



S-Fig. 3. **Low-risk comparison.** HA sequence comparison with dominant frequency human strains (A/Togo/0172/2021, A/Bangladesh/9004/2021, A/Wisconsin/04/2021) with Emergenet estimated H1N1 low-risk strain EPI2143526 (emergence score 5.66) showing substantially more differences compared to Extended Data Fig. 2.



S-Fig. 4. **E-distance validation in-silico using Influenza A sequences from NCBI database.** Panel a illustrates that the Emergenet induced modeling of evolutionary trajectories initiated from known haemagglutinin (HA) sequences are distinct from random paths in the strain space. In particular, random trajectories have more variance, and more importantly, diverge to different regions of the landscape compared to Emergenet predictions. Panels b-e show that unconstrained Q-sampling produces sequences maintain a higher degree of similarity to known sequences, as verified by blasting against known HA sequences, have a smaller rate of growth of variance, and produce matches in closer time frames to the initial sequence. Panel c shows that this is not due to simply restricting the mutational variations, which increases rapidly in both the Emergenet and the classical metric.

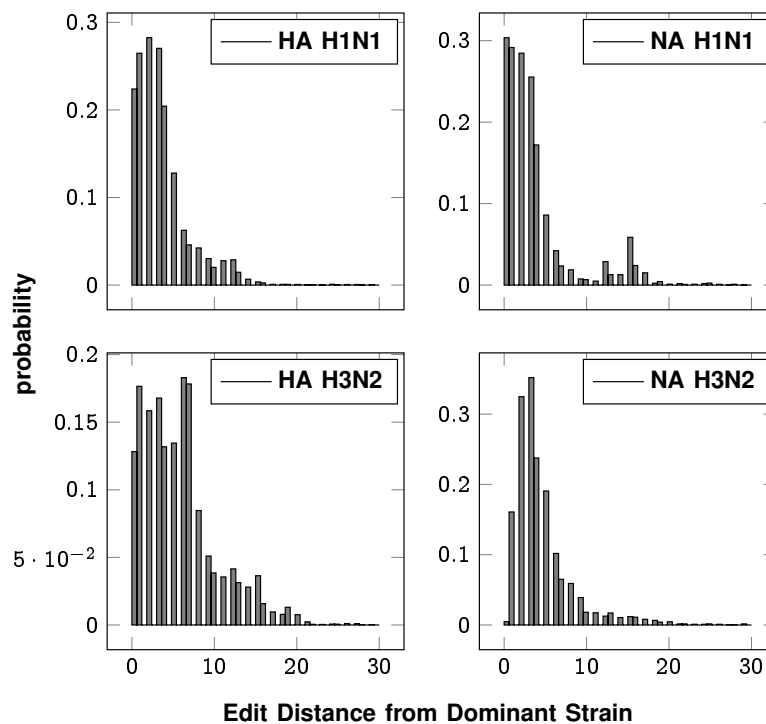


S-Fig. 5. **Sampling effects on E-distance.** We trained 100 Emergenet models the HA segment with different random samples of 3000 strains. We sample a pair of random strains from each of the two largest clusters and compute their E-distance under each Emergenet model. There is little to no overlap between the same cluster E-distances and the inter-cluster distances.

S-Tab. 4
 IRAT predictions that broadly corroborated with outbreaks

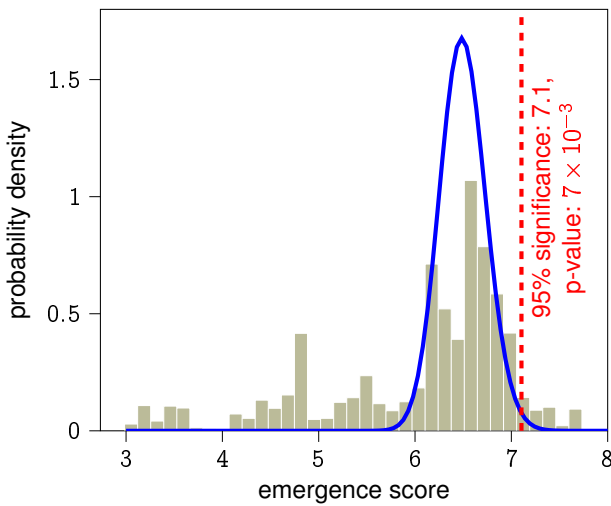
Influenza Virus	Subtype	IRAT Emergence Score	IRAT Impact Score	Description
A/swine/Shandong/1207/2016	H1N1	7.5	6.9	Cases of ILI (Influenza-like-illness) saw a substantial increase in weekly cases in the Shandong province of China during the years 2016-2017 when compared to previous years ⁶¹ . This strain was also chosen as a representative strain in a study by Sun, et al. which found that its potential for human infectivity "greatly enhances the opportunity for virus adaptation in humans and raises concerns for the possible generation of pandemic viruses" ⁶² .
A/Ohio/13/2017	H3N2	6.6	5.8	The CDC reports that flu activity in the United States during the 2017–2018 season started to increase in November and was dominated by Influenza A (H3N2) viruses through February ⁶³ .
A/Hong Kong/125/2017	H7N9	6.5	7.5	The CDC reports that "during March 31, 2013–August 7, 2017, a total of 1,557 human infections with Asian H7N9 viruses were reported; at least 605 (39%) of these infections resulted in death." 759 of these infections were reported during the fifth epidemic (October 1, 2016–August 7, 2017) ⁶⁴ .

a. Distribution around dominant strain

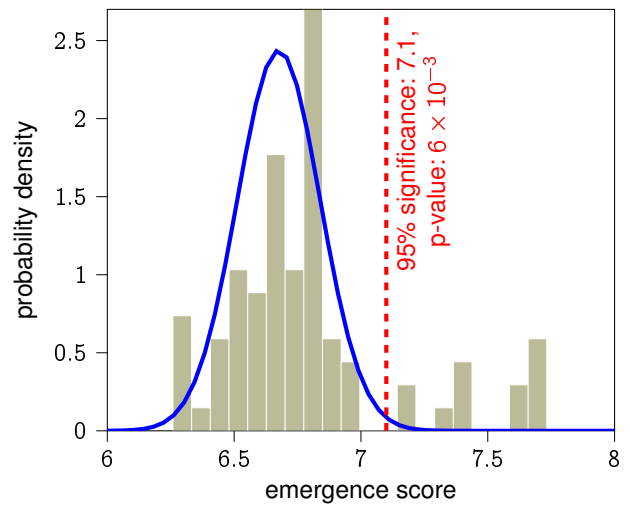


S-Fig. 6. **No. of mutations from a seasonal dominant (maximal frequency) strain over the years** The quasispecies that circulates each season for each sub-type is tightly distributed around the maximal strains on average.

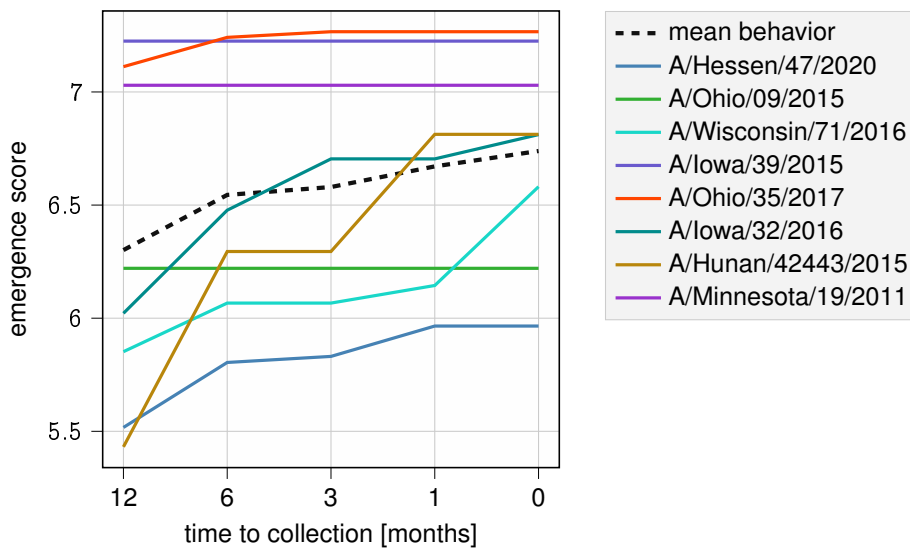
a. All animal strains
(normal dist. fitted to values > 6.25)



b. Strains > 6.25 unique up to 15 edits



S-Fig. 7. Distribution of Emergenet predicted emergence scores for animal strains. Panel a We plot the computed emergence risk score distribution of 6,354 animal strains collected post-2020. **Panel b** We show the distribution of computed emergence scores only for strains which are unique up to 15 edits in their HA sequence. Note that the right tail, where the high risk strains lie, are extreme occurrences in a statistically significant sense with p-values lower than 0.01.



S-Fig. 8. Emergenet predicted risk scores for top 8 risky variant strains. We evaluate H1N1 and H1N2 animal strains that emerged in humans with Emergenet at twelve, six, three, one, and zero months before their collection date, showing how often risk can be observed to increase over time.

S-Tab. 5
Emergence score estimations for fifteen H1N1 and H1N2 variant strains (animal strains collected in humans)

Variant strain	Subtype	12 months prior	6 months prior	3 months prior	1 month prior	At collection
A/Ohio/24/2017	H1N2	7.5	7.6	7.6	7.6	7.6
A/Ohio/35/2017	H1N2	7.1	7.2	7.3	7.3	7.3
A/Iowa/39/2015	H1N1	7.2	7.2	7.2	7.2	7.2
A/Minnesota/19/2011	H1N2	7.0	7.0	7.0	7.0	7.0
A/Hunan/42443/2015	H1N1	5.4	6.3	6.3	6.8	6.8
A/Iowa/32/2016	H1N2	6.0	6.5	6.7	6.7	6.8
A/Wisconsin/71/2016	H1N2	5.8	6.1	6.1	6.1	6.6
A/Ohio/09/2015	H1N1	6.2	6.2	6.2	6.2	6.2
A/Michigan/383/2018	H1N2	4.5	5.2	6.1	6.1	6.1
A/Hessen/47/2020	H1N1	5.5	5.8	5.8	6.0	6.0
A/Wisconsin/03/2021	H1N1	5.9	5.9	5.9	5.9	5.9
A/California/71/2021	H1N2	5.3	5.3	5.4	5.5	5.5
A/Netherlands/10370-1b/2020	H1N1	5.0	5.0	5.0	5.0	5.0
A/Netherlands/3315/2016	H1N1	3.3	4.1	4.1	4.1	4.3
A/Bretagne/24241/2021	H1N2	4.2	4.2	4.2	4.2	4.2

S-Tab. 6
High risk strain percentage comparison between variant pool and animal surveillance

Emergence score thresholds	6.0	6.5	6.8	7.0	7.1
% in variants	60.0	46.7	40.0	26.7	20.0
% in animal surveillance	69.1	45.5	18.5	6.4	5.6

S-Tab. 7
 General linear model for evaluating effect of data diversity on Emergenet performance

Variable Name	Description
enet_complexity	Cumulative number of nodes in all predictors in the corresponding Emergenet
data_diversity	Number of clusters in set of input sequence where each sequence in a specific cluster is separated by at least 5 mutations from sequences not in the cluster
ldistance_WHO	Deviation of WHO predicted strain from the dominant strain

model:dev ~ enet_complexity + data_diversity + enet_complexity * data_diversity + ldistance_WHO
 Generalized Linear Model Regression Results

```

=====
Dep. Variable:          dev      No. Observations:          235
Model:                  GLM      Df Residuals:            230
Model Family:          Gaussian  Df Model:                 4
Link Function:         identity  Scale:                    23.214
Method:                 IRLS     Log-Likelihood:          -700.43
Date:                   Thu, 11 Jun 2020  Deviance:                 5339.2
Time:                   16:45:46   Pearson chi2:            5.34e+03
No. Iterations:        3          Covariance Type:        nonrobust
=====

```

	coef	std err	z	P> z	[0.025	0.975]
Intercept	-0.1116	1.090	-0.102	0.918	-2.248	2.025
enet_complexity	0.0005	0.000	1.075	0.282	-0.000	0.001
data_diversity	0.3197	0.126	2.531	0.011	0.072	0.567
enet_complexity:data_diversity	-6.932e-05	5.01e-05	-1.383	0.167	-0.000	2.89e-05
ldistance_WHO	-0.0348	0.035	-1.007	0.314	-0.102	0.033

model:dev ~ enet_complexity + data_diversity + ldistance_WHO
 Generalized Linear Model Regression Results

```

=====
Dep. Variable:          dev      No. Observations:          235
Model:                  GLM      Df Residuals:            231
Model Family:          Gaussian  Df Model:                 3
Link Function:         identity  Scale:                    23.306
Method:                 IRLS     Log-Likelihood:          -701.41
Date:                   Thu, 11 Jun 2020  Deviance:                 5383.6
Time:                   16:45:47   Pearson chi2:            5.38e+03
No. Iterations:        3          Covariance Type:        nonrobust
=====

```

	coef	std err	z	P> z	[0.025	0.975]
Intercept	1.0841	0.665	1.630	0.103	-0.219	2.387
enet_complexity	-4.12e-05	0.000	-0.156	0.876	-0.001	0.000
data_diversity	0.1788	0.075	2.392	0.017	0.032	0.325
ldistance_WHO	-0.0695	0.024	-2.930	0.003	-0.116	-0.023